Politecnico di Torino

Politecnico di Torino

Dipartimento di Ingegneria Meccanica e Aerospaziale

Master degree course in Aerospace Engineering

Master Degree Thesis

RAMS estimation of hybrid-electric aircraft propulsion architectures

Candidate:
Leonardo Checcucci
Matr. n. 301590

Supervisor:
Professor Marco Fioriti

JULY 2023

A mia Madre e mio Padre, che hanno sempre creduto e sopportato tutte le mie scelte

Abstract

It is a truth universally acknowledged that we are living in a very important period in the area of climate change. The effects of greenhouse gas emissions and pollutants are manifesting themselves with greater frequency and intensity than ever before, and as a result, the world is moving in a more environmentally sustainable direction. This implies that the aviation sector is also studying solutions to reduce greenhouse gases.
The aim of this thesis is to show the reader the reliability aspect of new turbo-electric and turbo-hybrid architectures, as well as the current state of the art of such technologies that various companies and universities are studying and developing.
In order to do this, designs were analysed that were both at an advanced stage of study and of relative importance in terms of possible application. The analysis was carried out by creating Reliability Block Diagrams of these architectures (based on available information), where each block represents a component/sub-system with its relative reliability value, which in turn was derived from their failure rates.
Once the failure rate of the system under consideration has been derived, it is compared with the values of current commercial aircraft. In general, the comparison shows that many of these architectures are not yet mature and the failure rates differ from current aircraft by as much as 6/7 orders of magnitude. This is due to the fact that the architectures are generally more complex and also because they use technologies that are either in the development phase or, if they exist, have not yet realised the aeronautical version. The only exception is the STARC-ABL programme, which carries a more conservative architecture and is realised with all existing technologies.

Aknowledgements

La prima persona a cui devo la mia più sincera gratitudine è il mio Tutor Professore Dottor Marco Fioriti, che con la sua professionalità, dedizione, motivazione e continuo coinvolgimento, mi ha guidato nella realizzazione di questa Tesi.
Un grazie pieno di affetto alle Monache del Monastero di Santa Lucia di Trevi per la loro costante e amorevole presenza nella mia vita e nella mia crescita.
Ringrazio mia cugina Nicole Bonamici, co-fondatrice e CEO di Edralon, per la sua carica positiva e incitamento nel mio percorso di studi.
Un ringraziamento a Umberto Nazzareno Tonti, Presidente della OMA S.P.A., per la costruttiva competenza che mi è stata da riferimento.
Alla mia "Famiglia" di Torino Giuseppe, Marco, Luca, Danilo, Salvatore, Emeric, Laura e Martina, con cui ho condiviso la maggior parte delle sfide di questa avventura magistrale.
Grazie ai miei amici fraterni Stefano e Jacopo Bocci per gli aiuti informatici fondamentali per i miei studi universitari.
Ai miei amici Andrea, Giorgia, Margherita, Sara, Davide, Francesco, Amedeo, Veronica e Giulio, con i quali condivido sempre con entusiasmo ogni passo della nostra vita.
Grazie a Riccardo, Jacopo, Niccolò, Lodovico, zia Paola, zio Enzo e zio Bruno, per il grande affetto che mi accompagna e mi sostiene sempre.

Index

Abstract I

Aknowledgements II

List of Figures V

List of Tables VIII

Nomenclature IX

1 Introduction 1
- 1.1 Background . . . 1
- 1.2 Objective . . . 2

2 Architecture 4
- 2.1 Full Electric Architecture . . . 4
- 2.2 Turbo-Electric Power Controlled e Direct . . . 6
- 2.3 Turbo Hybrid Series/Parallel . . . 9
  - 2.3.1 T.H. Series . . . 9
  - 2.3.2 T.H. Parallel . . . 13
- 2.4 Batteries Fuel Cells . . . 15

3 Reliability Block Diagram Study 19
- 3.1 N3-X . . . 20
- 3.2 SUGAR VOLT . . . 31
- 3.3 X-57 MAXWELL . . . 34
- 3.4 DRAGON ONERA . . . 38
- 3.5 STARC-ABL . . . 46
- 3.6 PEGASUS NASA . . . 48

4 NPRD Quaternion data interpretation 52
- 4.1 NPRD study . . . 52
- 4.2 Data Analysis . . . 56
  - 4.2.1 Motors . . . 56

4.2.2 Fuel system 57
4.2.3 Mechanical parts 57
4.2.4 Electrical parts 58

5 Global Analysis 60

6 Conclusions 64

A Appendix 66
A.1 CONVENTIONAL CONFIGURATIONS 66
A.1.1 Series Diagram 66
A.1.2 Parallel Diagram 67
A.2 UNCONVENTIONAL CONFIGURATIONS 67
A.2.1 H-pattern 67
A.2.2 S-pattern 69
A.2.3 R-pattern 69
A.2.4 V-pattern 71

Bibliography 72

List of Figures

1.1 "La France" - Methods dor the Design and Evolution of Future Aircraft, Technische Universitat Munchen - 2015 2

1.2 "Solar Riser" - Methods dor the Design and Evolution of Future Aircraft, Technische Uni-versitat Munchen - 2015 2

2.1 "Configuration Diagram Full Electric" - System Analysis of Turbo-Electric and Hybrid Electric Pro-pulsion Systems on a Regional Aircraft – 2018 4

2.2 "E-Fan 2.0" - EV Aircraft Archives, LECCAR - 2015 5

2.3 "X-57 Maxwell Control Concept of Operations" - System-Level Control Concepts for Electrified Aircraft Propulsion Systems – 2021 . . . 6

2.4 "Configuration Diagram Turbo Electric Power Controlled" - System Analysis of Turbo-Electric and Hybrid Electric Pro-pulsion Systems on a Regional Aircraft – 2018 6

2.5 "Configuration Diagram Turbo Electric Direct" - System Analysis of Turbo-Electric and Hybrid Electric Pro-pulsion Systems on a Regional Aircraft – 2018 7

2.6 "Preliminary Cross-redundant Architecture Diagram" - Multi- disciplinary Design and performance of the ONERA Hybrid Electric Distributed Propulsion concept (DRAGON) – 2020 8

2.7 "STARC-ABL Control Concept of Operations" - System-Level Control Concepts for Electrified Aircraft Propulsion Systems – 2021 . . . 9

2.8 "Configuration Diagram Turbo Hybrid Series" - System Analysis of Turbo-Electric and Hybrid Electric Pro-pulsion Systems on a Regional Aircraft – 2018 10

2.9 "NX-3 Control Concept of Operations" - System-Level Control Concepts for Electrified Aircraft Propulsion Systems – 2021 11

2.10 "Proposed all electric NASA N3-X aircraft EPS" - DC Load Flow Models for the Electric Power System of Wide Body All Electric Aircraft – 2022 12

2.11 "Configuration Diagram Turbo Hybrid Parallel" - System Analysis of Turbo-Electric and Hybrid Electric Pro-pulsion Systems on a Regional Aircraft – 2018 13
2.12 "SUGAR Volt Control Concept of Operations" - System-Level Control Concepts for Electrified Aircraft Propulsion Systems – 2021 . . . 14
2.13 "PEGASUS NASA Control Concept of Operations" - System-Level Control Concepts for Electrified Aircraft Propulsion Systems – 2021 . 15
2.14 ≪Hydrogen fuel cells, explained≫-Airbus-15/10/2020. 17

3.1 ≪Multifeeder Architecture Diagram with Component Naming Convention≫ - Architecture, Voltage, and Components for a Turboelectric Distributed Propulsion Electric Grid Final Report - 2015 20
3.2 ≪Simplified diagram of the N3-X architecture≫ - 2023 21
3.3 ≪N3-X Logistic RBD≫ - 2023 22
3.4 ≪N3-X Simplified Safety RBD≫ - 2023 23
3.5 ≪N3-X Complete Safety RBD≫ - 2023 24
3.6 ≪N3-X Complete Cruise RBD≫ - 2023 28
3.7 ≪N3-X Cruise RBD≫ - 2023 29
3.8 ≪SUGAR VOLT Safety RBD≫ - 2023 32
3.9 ≪Turbofan engine scheme with electric-assisted propulsion≫ - Performance analysis of an electrically assisted propulsion system for a short-range civil aircraft - 2019 33
3.10 ≪SUGAR VOLT Cruise RBD≫ - 2023 34
3.11 "X-57 Maxwell Control Concept of Operations"- SCEPTOR Power System Design:Experimental Electric Propulsion System Design and Qualification for Crewed Flight Testing - 2016 35
3.12 ≪X-57 MAXWELL Security RBD vr.1≫ - 2023 36
3.13 ≪X-57 MAXWELL Security RBD vr.2≫ - 2023 36
3.14 ≪DRAGON Simplified Safety RBD≫ - 2023 39
3.15 ≪DRAGON Complete Safety RBD≫ - 2023 40
3.16 ≪DRAGON Complete Cruise RBD≫ - 2023 44
3.17 ≪DRAGON Cruise RBD≫ - 2023 45
3.18 ≪STARC-ABL Cruise RBD≫ - 2023 47
3.19 ≪PEGASUS Safety RBD≫ - 2023 49
3.20 ≪Mission Thrust Profile≫ - Analysis of the Parallel Electric-Gas Architecture with Synergistic Utilization Scheme (PEGASUS) Concept - 2019 49
3.21 ≪PEGASUS Cruise RBD≫ - 2023 51

4.1 NPRD window 53
4.2 NPRD filtre page 53

4.3 NPRD filtre aeronautical types 54
4.4 NPRD example page with the values 55

A.1 Series Diagram 66
A.2 Parallel Diagram 67
A.3 H-pattern 67
A.4 H-pattern when the H component always works and when it doesn't . 68
A.5 S-pattern 69
A.6 R-pattern 69
A.7 V-pattern 71

List of Tables

3.1 ≪N3-X Subsystems/Components Reliability≫ - 2023 22
3.2 ≪SUGAR VOLT Subsystems/Components Reliability≫ - 2023 31
3.3 ≪X-57 MAXWELL Subsystems/Components Reliability≫ - 2023 . . . 35
3.4 ≪DRAGON Subsystems/Components Reliability≫ - 2023 39
3.5 ≪STARC-ABL Subsystems/Components Reliability≫ - 2023 46
3.6 ≪PEGASUS NASA Subsystems/Components Reliability≫ - 2023 . . . 48

4.1 ≪Motors reliability≫ - 2023 56
4.2 ≪Fuel system's parts reliability≫ - 2023 57
4.3 ≪Mechanical parts reliability≫ - 2023 57
4.4 ≪Electrical parts reliability≫ - 2023 58

5.1 ≪Architectures Failure Rate≫ - 2023 *This is the value of when you can counteract the yawing moment with aerodynamic surfaces. The value if this moment is not counteracted is $7{,}44 \cdot 10^{-5}$. **This is the value you would get with a hybridisation of 50% of cruising engines. In the case of a 25% hybridisation, this is based on that of the turboprop; in the case of a 75% hybridisation, the value is $6{,}44 \cdot 10^{-5}$. 60

Nomenclature

CO_2 = Carbon Dioxide
NO_x = Nitrogen Oxides
RAMS = Reliability Availability Maintainability Safety
V = Volt
Wh = Watt per hour
nm = nautical miles
km = kilometres
kg = kilogram
PSC = Propulsion Supervisory Control
AC = Alternate Current
DC = Direct Current
SC = Supervisory Control
MTOW = Maximum Take-Off Weight
HP = Horse Power
BED = Battery Energy Density
PEM = Proton Exchange Menbrane
$SOFC_S$ = Solid Oxide fuel cells
RBD = Reliability Block Diagram
FR = Failure Ratio
R = Reliability
t = Time (hour)
OEI = One Engine Inoperative
NPRD = Nonelectronic Parts Reliability Data

Chapter 1

Introduction

1.1 Background

The aviation sector is responsible for 12% of CO_2 emissions in the transport sector, where for example, it emitted 859 million tons in 2017 [1]. As a result, various political and social bodies are promoting environmental policies all over the world towards a greener direction, although the reduction of emissions of CO_2 and NO_x due to the nature of our sector must be accompanied by low costs, by performance, if not superior, at least equal to modern technologies and above all by the same safety standards.
Solutions aimed at reducing pollutant emissions involve electrifying the drive system, leading to Full Electric, Turbo Electric and Turbo Hybrid architectures.
Research in the field of electric propulsion is nothing new for the aeronautical world. In fact, since the end of the 19th century, efforts were already being made to create electrically powered aircraft, such as the airship 'La France' [2]. But then with the development first of reciprocating engines and then of jet engines, which provided better performance and lower manufacturing costs, the development of electric propulsion in aviation was abandoned until the 1970s. From this time, prototypes of electrically powered aircraft began to be built, such as the 'Solar Riser' built by Lerry Mauro, who flew it in 1979.

As anticipated, in recent years there has been a worldwide boost of environmental policies that various institutions are promoting. For example, Europe is following the Flightpath 2050, promoted by the EU, which envisages the reduction by 2050 of CO_2 emissions in aviation by 75%, of NO_x by 90% and of noise pollution by 65% [3][4]. Similarly, in America, the N+ plan promoted by NASA (National Aeronautics and Space Administration) is being followed, where in the N+3 configuration (2025) they envisage a 74% reduction in NO_x emissions and a 70% reduction in fuel consumed [5].

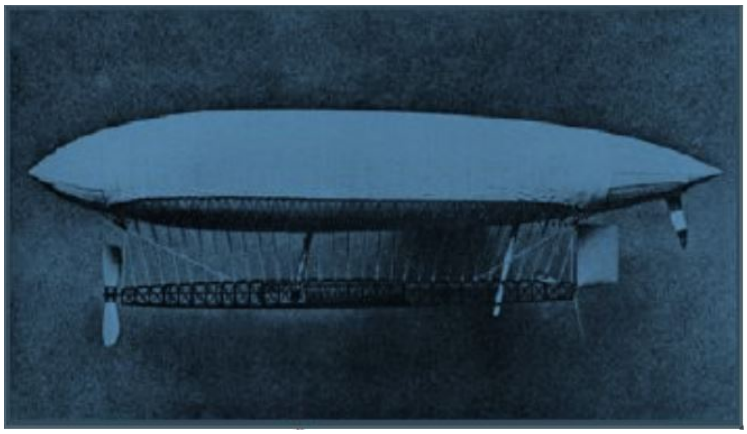

Figure 1.1: "La France" - Methods dor the Design and Evolution of Future Aircraft, Technische Universitat Munchen - 2015

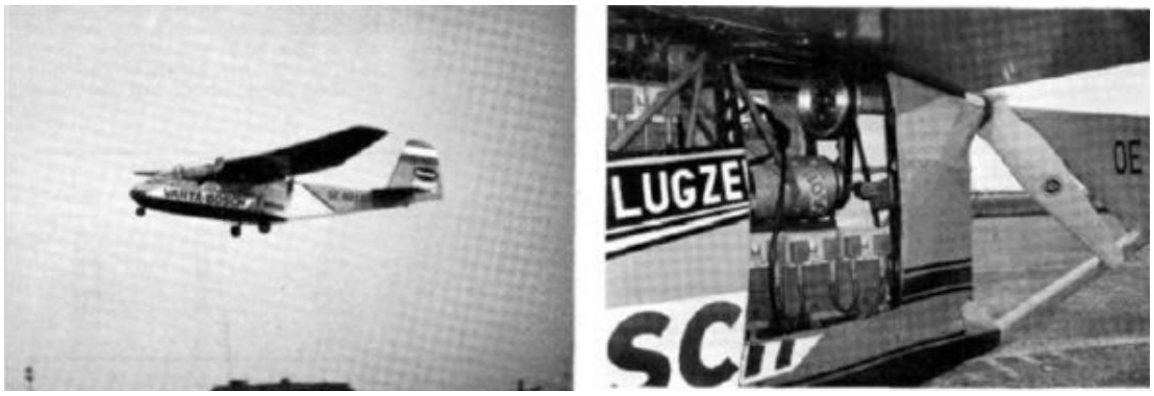

Figure 1.2: "Solar Riser" - Methods dor the Design and Evolution of Future Aircraft, Technische Uni-versitat Munchen - 2015

Thanks to these policies, there has been a huge increase in projects aimed at the electrification of aircraft and beyond, such as the production of biofuels, a topic not covered in this thesis.

1.2 Objective

The purpose of this thesis is the analysis and study at RAMS (Reliability Availability Maintainability Safety) level of turbo electric/hybrid technologies, so as to indicate which paths will be pursued in the future.
The analysis includes a description of the main architectures with examples of projects carried out worldwide by leading companies in the sector and universities. At this point, the projects that are at a sufficiently advanced stage of development to allow a reliability study using the Reliability Block Diagram (RBD) method are analysed.
From this study, the resulting values are compared with the current technologies used, showing in general the goodness of these designs, although the components

used must have further analysis for their failure rate values. In fact, since many of the technologies used are still in the development phase, the failure rate values, if there was no dedicated research, were derived by association with real components even if they were not specifically used for aviation.
Quaternion's NPRD databook was used to derive the failure rates, where probabilistic models were used to derive these values, trying to make estimates as realistic as possible.

Chapter 2

Architecture

In this chapter, the different propulsion architectures will be analysed with examples and diagrams.

2.1 Full Electric Architecture

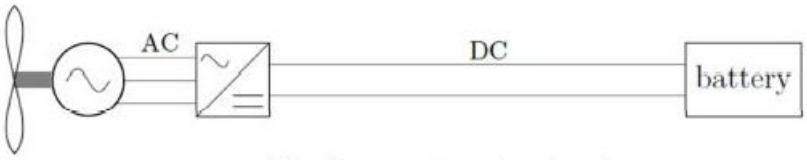

Figure 2.1: "Configuration Diagram Full Electric" - System Analysis of Turbo-Electric and Hybrid Electric Pro-pulsion Systems on a Regional Aircraft – 2018

Before discussing the various turbo/hybrid configurations, it is appropriate to discuss the Full Electric architecture.
This construction involves battery packs and/or fuel cells that supply direct current and are followed by an inverter that transforms the current from direct to alternating current, so that an electric motor can drive the propeller/fan.
Its great merits are that it does not directly emit CO_2 , NO_X and reduces aeroacoustic pollution. This makes this architecture the most suitable for aircraft that have to fly in urban areas (e.g. air taxi aircraft).
There are many studies and projects with this structure, such as:

- **E-FAN 2.0 Airbus**: Two-seater electric aircraft developed by Airbus and its patners, that was born as a demonstrator. It has two 60 kW electric motors powered by a 120-cell 250V lithium-ion battery. At take-off it reaches 110 $\frac{km}{h}$, at cruise 160 $\frac{km}{h}$ and at maximum speed 220 $\frac{km}{h}$ [6].

Figure 2.2: "E-Fan 2.0" - EV Aircraft Archives, LECCAR - 2015

- **Pantera Pipistrel**: Four-seater electric aircraft developed by the company Pipistrel. In addition to the electric version, it can also be powered by a hybrid and a conventional one (Lycoming IO-540V-V4A5 engine), although the only one on the market is the conventional one. The electric motor will have 200 kW of power at take-off [7].

- **Alice Eviation Aircraft**: 12-seat electric aircraft developed by Eviation Aircraft. Equipped with two Magnix Magni650 electric motors with a power output of 700 kW each. The aircraft has a take-off weight of 8,346 kg, a range of 250 nm (463 km) and a top speed of 482 $\frac{km}{h}$. It is also powered by lithium-ion batteries [8].

- **ZeroAvia**: Company developing electric aircraft powered by Fuel Cells. These made their first flight test in January this year (2023) [9] [10].

- **X-57 maxwell**: It is a NASA demonstrator as part of the SCEPTOR project and aims to prove that a distributed engine configuration is 3.5 times more efficient than the reference aircraft, a Tecnam P2006T.[11].
  Propulsion is all-electric and sees two motors in the wing tip sized for the cruise phase of the misson, plus 12 electric motors distributed in the rest of the wings (6 per side) to give extra power for take-off and climb. All the power required to operate these motors comes from two battery packs [12].

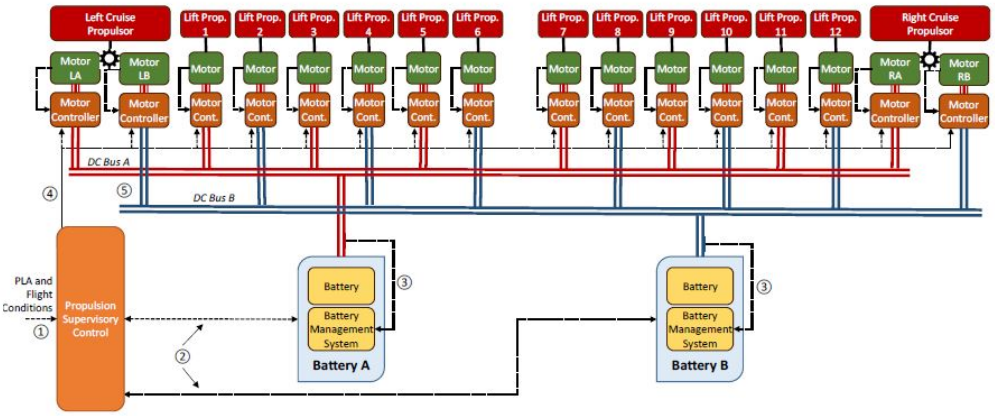

Figure 2.3: "X-57 Maxwell Control Concept of Operations" - System-Level Control Concepts for Electrified Aircraft Propulsion Systems – 2021

In general, the architecture sees upstream the Propulsion Supervisory Control, which receives as input information from on-board commands, the external environment and the state of charge of the batteries. As output, it sends control signals to the batteries and commands to the motor controller, which has the task of alternating the electrical energy coming from the batteries and modulating it according to the input from the PSC. The motor block in turn consists of the electric motor itself and the propellers. The battery packs consist of four battery modules plus a Battery Management System that has input from the buses that transmit the current to the motors, so that the supply voltage is kept constant. Each battery pack powers the two cruise motors plus 6 of the 12 boost motors [12].

2.2 Turbo-Electric Power Controlled e Direct

In general, the turbo-electric architecture is based on the diesel train model, i.e. the generation of electrical energy via a generator powered by an engine that can be turboshaft or turbofan, so that the electric motors that run the propellers/fans are powered by this.

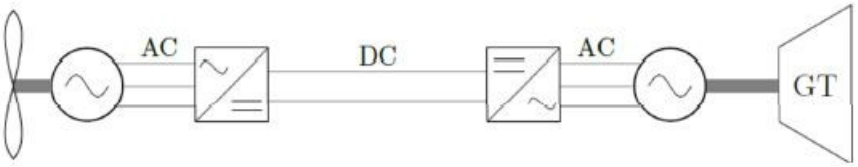

Figure 2.4: "Configuration Diagram Turbo Electric Power Controlled" - System Analysis of Turbo-Electric and Hybrid Electric Pro-pulsion Systems on a Regional Aircraft – 2018

With turbo-electric power control, the combustion engine is directly connected to the AC generator, where the generated current is then immediately rectified to DC. This is done because in this condition there are fewer conduction losses and, above all, when the inverter is used to switch it back to AC, it is possible to modulate the current to control the rotation of the electric motor and thus the propeller/fan, so as to control the power output.

Figure 2.5: "Configuration Diagram Turbo Electric Direct" - System Analysis of Turbo-Electric and Hybrid Electric Pro-pulsion Systems on a Regional Aircraft – 2018

Whereas with turbo-electric direct, a gearbox, which is placed between the combustion engine and the alternating current generator, is used to control the rotation of the electric motor. The function of the gearbox is to mechanically change the rotational speed at the output of the combustion engine shaft, so that the current produced by the generator is also modulated. This makes it possible to avoid switching to direct current.
Many studies exist for both configurations, the most relevant of which are listed below:

- **DRAGON ONERA**: The project is part of the European Clean Sky 2 programme. It envisages distributed turbo electric propulsion. They initially considered using Fuel Cells as energy generators, but this would have increased the technical difficulties even more, which led them to choose the configuration mentioned above. The energy generators are 2 turboshafts and power 40 electric fans [13].

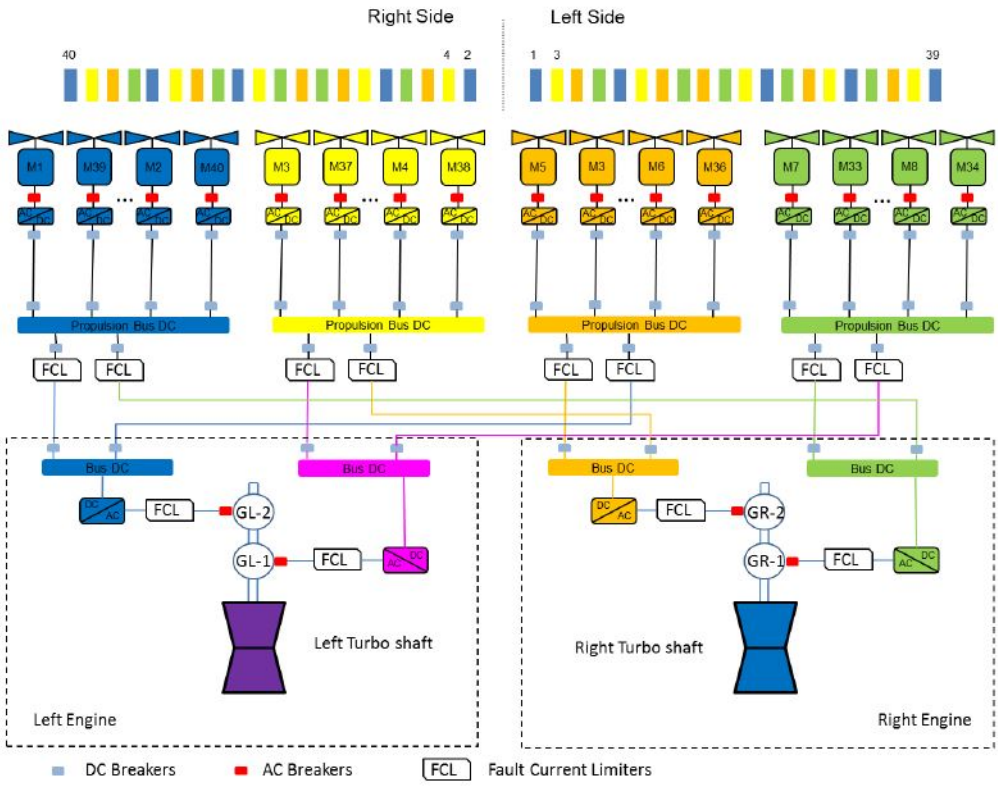

Figure 2.6: "Preliminary Cross-redundant Architecture Diagram" - Multi- disciplinary Design and performance of the ONERA Hybrid Electric Distributed Propulsion concept (DRAGON) – 2020

As can be seen from the figure 2.6 the two Turboshafts are connected to a gearbox, which feeds two alternators. The output alternating current is then rectified and this is sent to feed two of the four thruster buses, where one is the one used nominally, while the other serves as redundancy. The 10 associated electric fans are then fed from these buses. A further safety factor is the distribution of these fans, which are placed alternately in the wing, so as to ensure uniform thrust at all times [14].

- **Wright 1**: It is a 186-seater aircraft, developed in collaboration with EasyJet. It has a range of 1670 km and its configuration is C-wing. The thrusters are driven by an electric motor that can be powered either by batteries, fuel cells or a generator. [15].

- **STARC-ABL**: It is a NASA design of a 150-passenger aircraft with the single-aisle tube-and-wing concept. Its architecture makes it operate as if it were partially turbo-electric. The turbofans, which act as power generators in the cruise phase, generate 80 per cent of the thrust on take-off and 55 per cent on climb. The electric motor is positioned in the area usually occupied by the APU [16].

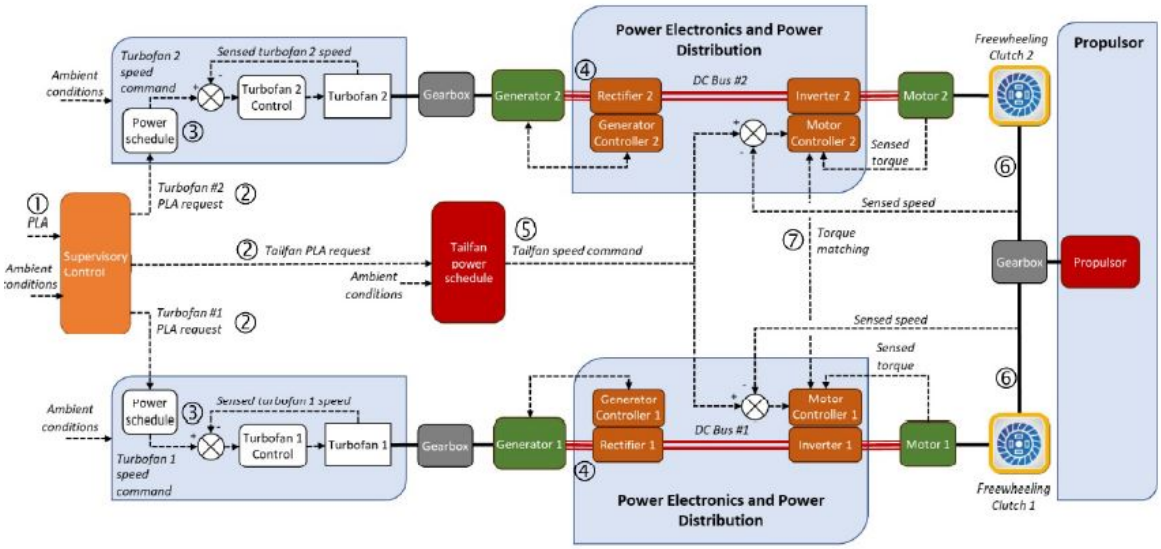

Figure 2.7: "STARC-ABL Control Concept of Operations" - System-Level Control Concepts for Electrified Aircraft Propulsion Systems – 2021

As can be seen in the figure 2.7 Supervisiory Control controls both turbofans and tailfans. To control the latter, input is first processed by the tailfan power schedule, from which there is then control action to the motor controller, which operates the alternator by bringing current from DC to AC. There must be torque matching between the motor controllers, so that the electric motors are coupled together. In the event of a failure of one of the two turbofans, in order to always take advantage of the turboelectric propulsion in cruise, a freewhell is placed between the electric motor and the tailfan gearbox so that the mechanical signal does not travel up the systems of the failed motor [12].

2.3 Turbo Hybrid Series/Parallel

The two configurations, the hybrid series and the hybrid parallel are very different.

2.3.1 T.H. Series

The Turbo Hybrid Series architecture is related to the turbo electric power controlled architecture and solves their great criticality, namely when a large amount of power is required from the electric motor in a relatively short time. To do this, a battery block is added. This block is recharged by the generator at times when the energy produced exceeds what is needed.
This architecture, being very similar to the power controlled one, has almost all its merits and shortcomings.

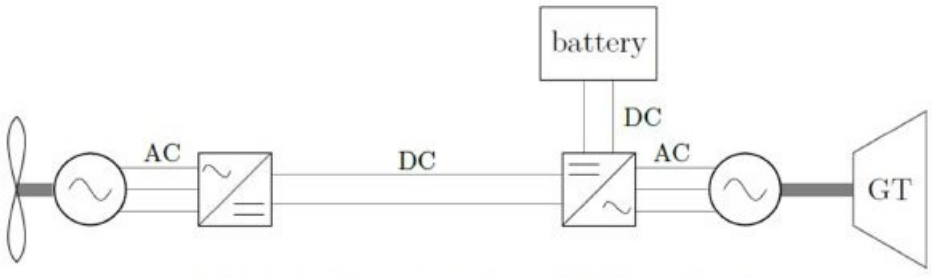

Figure 2.8: "Configuration Diagram Turbo Hybrid Series" - System Analysis of Turbo-Electric and Hybrid Electric Pro-pulsion Systems on a Regional Aircraft – 2018

Project examples of this configuration are:

- **N3-X NASA**: Aircraft designed by NASA for the study of turbo-electric propulsion distributed over the load-bearing section. In fact, the configuration of the aircraft is not the traditional one but a load-bearing fuselage. It has two turboshaft engines as power generators and this is distributed to the 16 small fans located on the wing via superconductors. The generators are placed at the wing tip where they operate at constant speed and use liquid hydrogen as fuel [17].

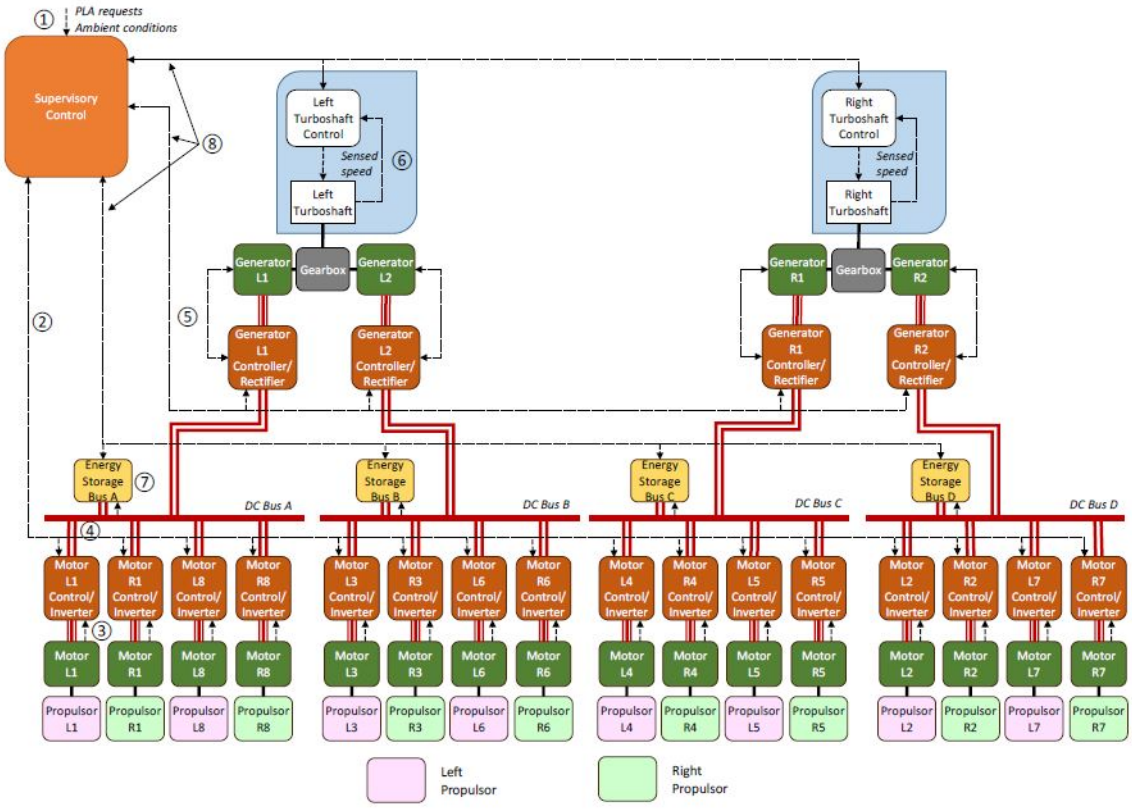

Figure 2.9: "NX-3 Control Concept of Operations" - System-Level Control Concepts for Electrified Aircraft Propulsion Systems – 2021

In general, the architecture consists of an SC that receives as data inputs from command, environmental conditions, and outputs from the various components of the turbo electric system. As output, it gives command actions to the same components mentioned above.

In order, each of the two turboshafts has a control computer that receives input from external commands and the shaft's rotational speed, so that it remains within the required parameters. This shaft is connected to a gearbox that feeds two alternating current generators. Rectifiers are positioned downstream so that the current changes from AC to DC. These controllers are obviously in communication with the upstream generators (at the control level) and receive directives from the SC. At the output of the rectifier you have a bus that feeds 4 of the 16 motors and a battery pack. From here the operation is the same as described in the X-57 Maxwell [12].

N3-X also has a full-electric version in the pipeline as shown in the figure below.

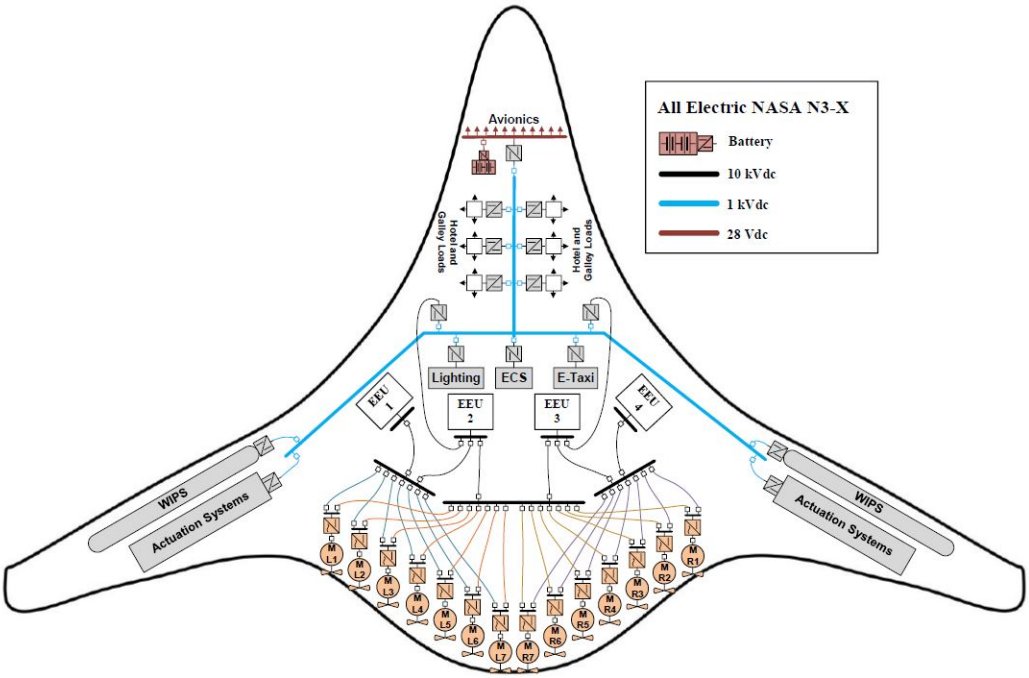

Figure 2.10: "Proposed all electric NASA N3-X aircraft EPS" - DC Load Flow Models for the Electric Power System of Wide Body All Electric Aircraft – 2022

- **ECO-150**: It is an ESAero project to build a B-737-class aircraft (around 150 on board) in a turbo-electric configuration with distributed thrusters. Two configurations were developed in this project, one with cryogenic cooling and the other without [18].
  At the level of propulsion architecture it is identical to the N3-X described above, although it is fair to say that ECO-150 at the structural level is like conventional aircraft [12].

- **IMOTHEP**: Avio's serial hybrid turbo engine project as part of the European IMOTHEP project, which is a four-year EU programme mainly aimed at researching these new architectures[19].

- **ZUNUM**: It was an American company that was designing a 12-seat regional turbo hybrid aircraft. The generator gave a power output of 500 kW, which with batteries came to a total of 1 MW. It would have had an MTOW of 5216 kg, a maximum range of more than 1200 km and a top speed of about 550 $\frac{km}{h}$ [20].

- **Efan-X**: It is a demonstrator built by the joint venture between Airbus and

Rolls-Royce. The programme involved replacing one of the engines in a four-engine aircraft with a 2 MW electric propeller. A serial turbo-hybrid architecture was developed to power it. However, the programme was cancelled in April 2020 due to the Covid-19 pandemic [21] [22].

- **e-Genius**: Two-seater aircraft with turbo hybrid propulsion architecture developed by the University of Stuttgart. The aircraft has a top speed of 230 $\frac{km}{h}$ and a range of 504 km. The university stated that the aircraft can consume less than 3 litres per 100 km at a cruising speed of 170 $\frac{km}{h}$ [23].

2.3.2 T.H. Parallel

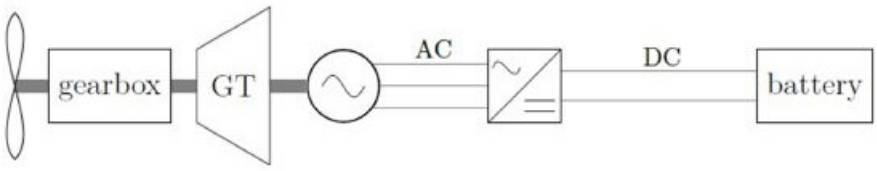

Figure 2.11: "Configuration Diagram Turbo Hybrid Parallel" - System Analysis of Turbo-Electric and Hybrid Electric Pro-pulsion Systems on a Regional Aircraft – 2018

On the other hand, the turbo hybrid parallel architecture exploits the concept of hybrid car engines, or rather, propulsion is provided by the classic engine unit (turbofan/prop) and an electric motor powered by batteries/fuel cells for better performance and/or lower pollutant emissions. From the picture it can be seen that the current released by the battery is direct current, which implies having an inverter to transform it into alternating current to provide additional power to the engine [24]. If there is, in a flight phase such as the descent before landing, a recovery of energy by the motor, the inverter must also function as a rectifier. This, however, only applies if energy is taken from the batteries alone [25].
This architecture makes it possible to reduce the size of the engines so that they are designed to have maximum power during the cruise phase, in contrast to what happens now where the engines are sized to have maximum power during the take-off phase. This is because the missing power is compensated for by the electric motor. From this statement it can be said that the phases in which the hybrid/electric part is used are taxi (full-electric), take-off and ascent (hybrid) and, as mentioned earlier, in the descent phase for partial recharging [26].
However, this architecture presents difficulties in the integration of the two energy sources both at the construction and control level.
In fact, the electric motor must be placed inside the motor (fan/prop) with all the

problems associated with space and maintaining operating conditions [26]. In addition, there is the problem of the throttle interface with these two energy sources, which is important for a uniform thrust response [25][26].
A positive note of this architecture is that no major structural changes are made to the aircraft, allowing it to enter the market in less time than other architectures[27]. This architecture led to the realisation of the following projects:

- **Project 804 X-plane**: A project by PrattWhitney and Collins Aerospace, which envisages the realisation of a parallel turbo-hybrid propulsion architecture, with a hybridisation of 50 %, i.e. of the total 2MW of power, half is provided by the electric component. This engine is mounted on a Bombardier Dash 8 Series Q100 in place of one of the two original engines. This aircraft will be flight-tested in 2024 [28].

- **SUGAR**: Ít is the turbo-electric engine research programme headed by Boeing together with General Electrics (GE) and the Georgia Institute of Technology. With the SUGAR VOLT project, they have developed two propulsion architectures with respect to NASA's N+3 standards: the 750 Balanced and the 750 Shutdown (the 750 stands for battery BED). Where the former has a 1380 HP electric motor and the latter a 7150 HP motor. In all, GE is developing its own version of the Balanced with a 1750 HP electric motor [29].

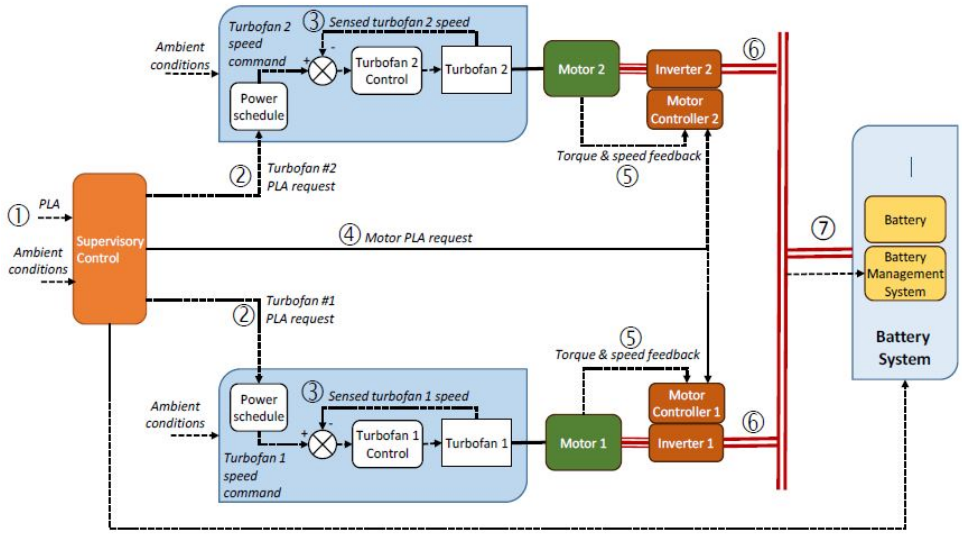

Figure 2.12: "SUGAR Volt Control Concept of Operations" - System-Level Control Concepts for Electrified Aircraft Propulsion Systems – 2021

In general, the aircraft is equipped with two turbofans powered by battery-powered electric motors, which operate on the low-pressure shaft of both turbofans. The SC controls the various subsystems. The input to the turbofans is

processed by a power schedule, which gives a speed command to the turbofan control. This input is added to the feedback coming directly from the engine. As far as the electrical section is concerned, there is a similarity to what was analysed previously, especially with the X-57 Maxwell [12].

- **PEGASUS NASA**: Ít is a 48-passenger aircraft based on the ATR-42. This design has the peculiarity of combining the two families of turbo-hybrid architectures, in fact it has two hybrid engines parallel to the wing tip, two electric engines placed closer to the wing root, and an electric engine in the tail of the aircraft. The turbo-hybrid motors will provide most of the thrust, while the electric motors give extra thrust in the take-off and climb phases, but will remain unused in the other phases of flight, where they can retract the propeller blades to avoid generating too much aerodynamic drag [30] [12].

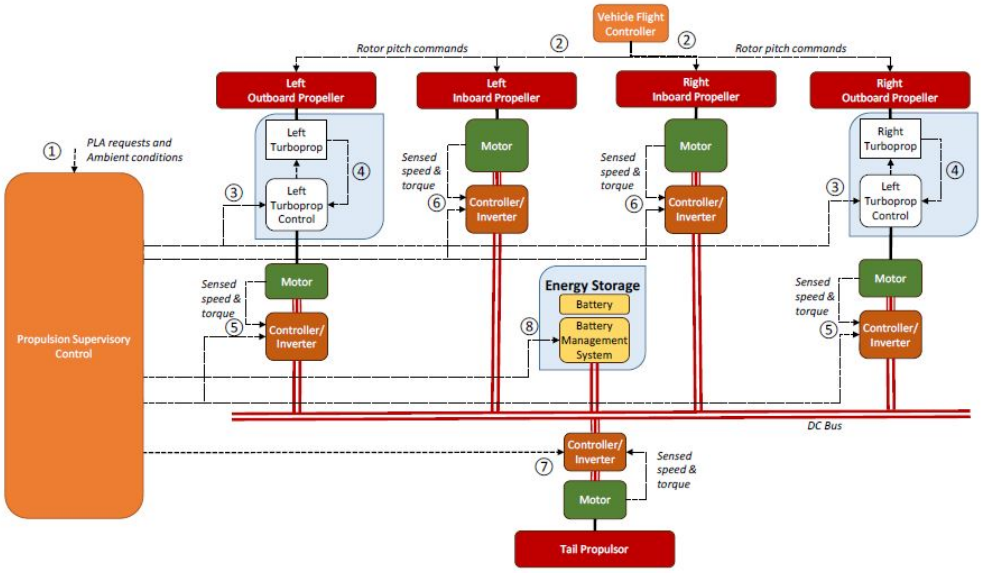

Figure 2.13: "PEGASUS NASA Control Concept of Operations" - System-Level Control Concepts for Electrified Aircraft Propulsion Systems – 2021

As already mentioned the architecture, given the previous designs, is a hybrid between the hybrid parallel and the series. Due to the turboprop engines, there is also the Vehicle Flight Controller, which controls the pitch of the propeller blades on the wings [12].

2.4 Batteries Fuel Cells

Before starting to deal with the reliability study of the architectures described above, it is necessary to delve into the state of the art of batteries and fuel cells, which

are a key component for the commercial success of these technologies. To do this, the following description is mainly based on the article [31].

Batteries offer the possibility of modular building blocks for a wide variety of operating concepts in centralised or distributed power systems. As mentioned above, batteries can respond very quickly to changing power demands and can be used to meet peak or load levelling requirements. Batteries provide electrical energy without direct CO_2 emissions, but one must take into account where the energy to charge them comes from and their life cycle.
Currently, lithium-ion batteries predominate on the market, which have a Battery Energy Density (BED) of between 100-200 $\frac{Wh}{kg}$. This density is very low compared to that of aviation fuels, which are generally around 13000 $\frac{Wh}{kg}$. Consequently, the effectiveness of batteries is closely linked to their development, where it is predicted that lithium-air batteries will reach a BED of around 11000 $\frac{Wh}{kg}$, which means that in the future at most they will be able to match the energy density of fuels.
Batteries also present a number of critical issues, such as equal weight with fuel will always have a lower or at most equal energy density, which means that more batteries (and therefore more mass) must be taken on board to have the same amount of energy available.
In addition, it must be taken into account that the energy output of batteries has a loss of charge, due to the inherent resistances it has [25]. Another aspect to consider is that the state of charge (an indicator of battery capacity) with continuous charge and discharge cycles has a decline [2]. In addition, there is the fact that temperature affects the battery system and the electrical system linked to the propulsion, so to avoid their failure and to achieve maximum performance, a range of operating temperatures must be ensured [2]. To do this, cryogenic cooling systems were also implemented.
To sum up, the cycles of batteries must be stable, because their charging capacity is not constant, but is a function of temperature and the number of cycles.
In addition, it must be taken into account that batteries can discharge automatically depending on the environment and other parameters [2].

Turning to fuel cells, their main characteristic is that they are not containers of energy, like batteries, but are an energy conversion system. In fact, they convert the chemical energy contained in the hydrogen molecule into electricity, which implies that the process is completely carbon free. In fact, the chemical reaction sees hydrogen as the fuel, oxygen (which is taken from the surrounding air) as the oxide, and the end result is water (as well as electricity).
A generic fuel cell is shown below:

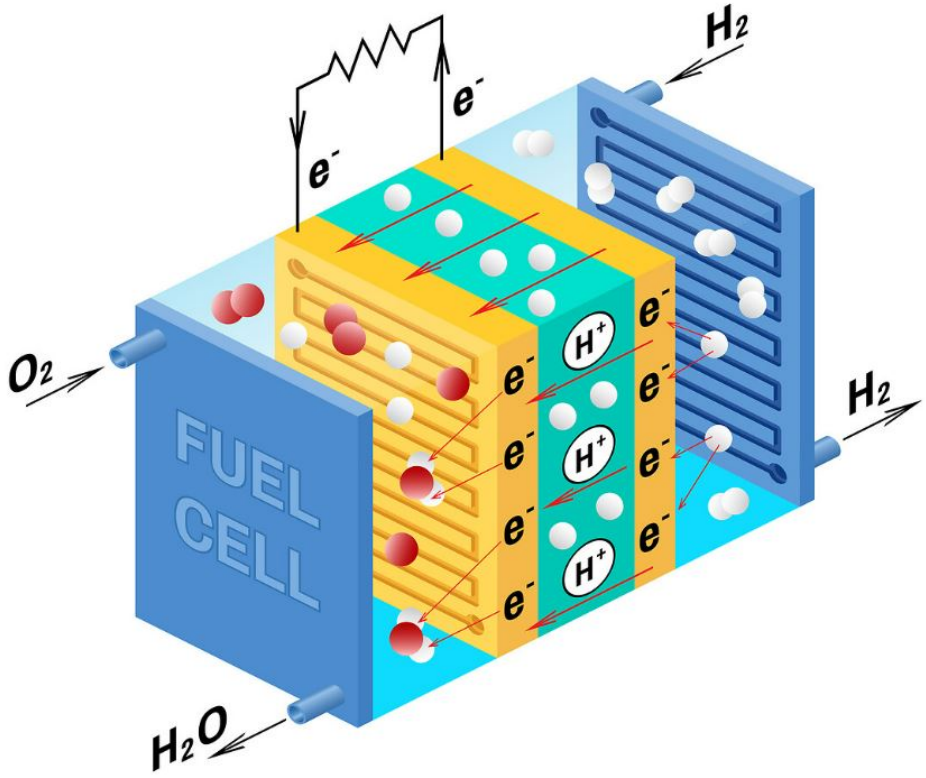

Figure 2.14: «Hydrogen fuel cells, explained»-Airbus-15/10/2020.

There are two types of fuel cells, developed for automotive transport: Proton Exchange Menbrane (PEM) fuel cells, which operate between 80° and 120° C and require pure hydrogen as fuel, and Solid Oxide fuel cells ($SOFC_S$), which operate between 750° and 1000° C where a variety of fuels (hydrocarbons) can be used, including jet fuels.
There are still no fuel cells certified for flight as both versions have technical difficulties that have yet to be resolved.
For the PEM there is the big problem of hydrogen storage, since it occupies large volumes for the same mass as a jet fuel. One could partially solve the bulk problem by using liquid hydrogen, but there is the problem of how to keep the hydrogen at cryogenic temperatures in flight. Not to mention that in general there are always huge losses of it due to its molecular size being extremely small 'no tank can hold it'.
For the $SOFC_S$, the storage problem is solved since the hydrogen used is taken from conventional fuels, although this results in CO_2 and NO_X emissions and, above all, very large operating temperatures, which leads to major problems in integrating the interface with the structure.

Regenerative fuel cells, which produce, store and then consume hydrogen, have also been considered for turbo-hybrid architectures, but these are much more complex than other fuel cells and have low energy efficiency.

Chapter 3

Reliability Block Diagram Study

At this stage, we proceed to study the reliability of the architectures presented in the previous chapter. To do this, it was decided to use the Reliability Block Diagram (RBD) tool, which logically relates the various systems (or subsystems/components depending on the detail of the analysis) in order to find the reliability of the machine as a whole. Usually the value with which this is expressed is the failure rate.
Before proceeding with the study, it is necessary to state that the analyses to follow will not take into account the cooling system of the components. The reason lies in the lack of studies concerning this fundamental aspect, since the cooling of electrical components is to be considered safety critical. As a result of the above, it is conceivable that the failure rates of the various architectures have higher values than reported.

3.1 N3-X

Based on document [32], we have the following aircraft propulsion system architecture:

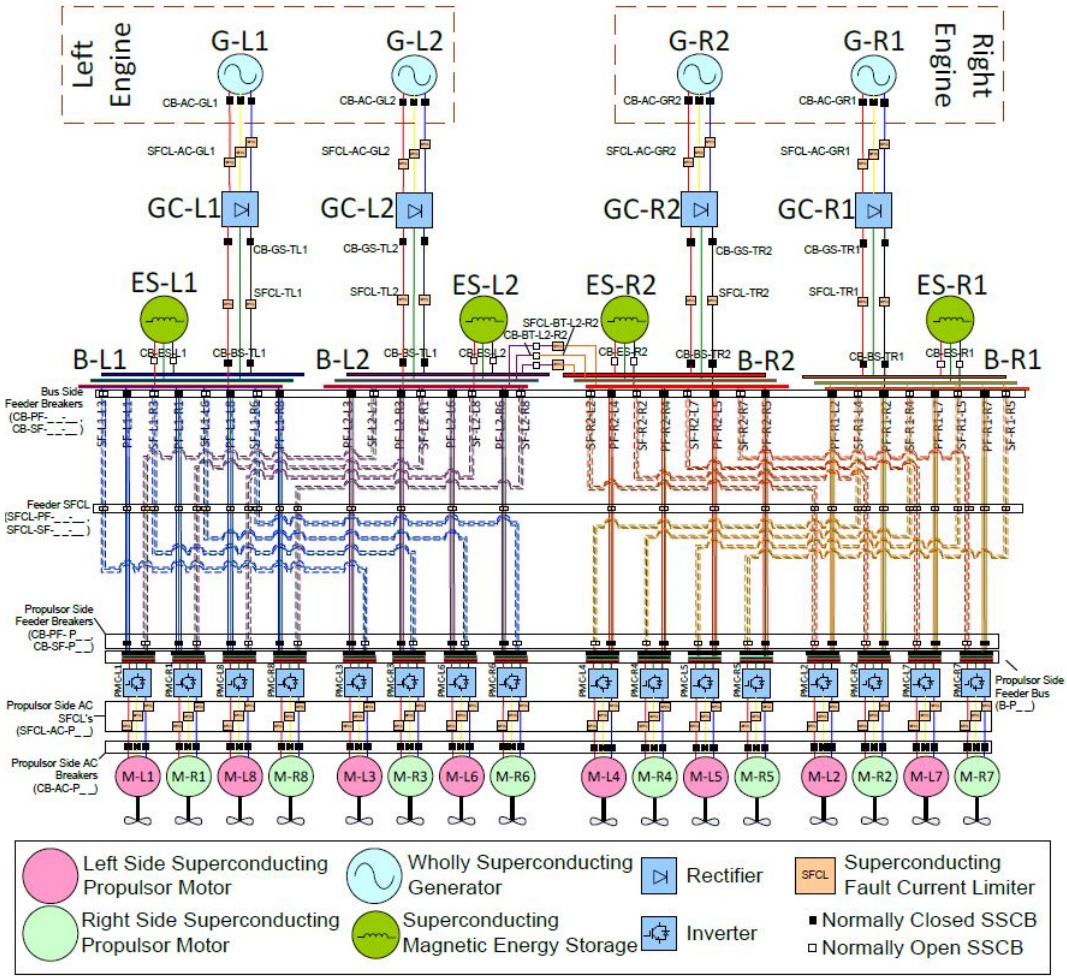

Figure 3.1: «Multifeeder Architecture Diagram with Component Naming Convention» - Architecture, Voltage, and Components for a Turboelectric Distributed Propulsion Electric Grid Final Report - 2015

This architecture is the result of a trade-off with other versions where performance and safety are optimised. In fact, based again on the study [32], it is possible to state that N3-X can guarantee flight performance with 8 of the 16 electric motors and with every second generator functioning.
In the image above, one can see what was said in the paper [12], on how at a high level the aircraft is organised (where, moreover, the detail of the electrical lines with their switches and fuses is added) and how the various redundancies of the electrical system are organised. It should also be noted that the electrical system uses cryogenic superconductors.
Having said this, given the level of the previous image, a simplified representation

of the system was made:

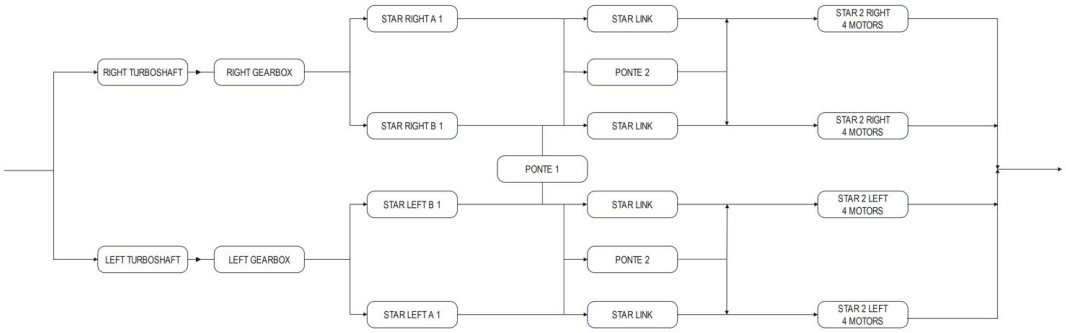

Figure 3.2: ≪Simplified diagram of the N3-X architecture≫ - 2023

Where STAR 1 means the electrical system from the AC generator (G in the first image) to the line bus, also considering the accumulators with their switches.
PONTE 1 represents the connection between the two buses B-L2 and B-R2; with STAR LINK we have the connection between the buses downstream of the generators and the buses located before the inverters in the case of normal operation, while with PONTE 2 we have the same connection, but redundant and coming from different buses. Finally, with STAR 2 you have the system running from the inverters up to the electric motor.
Obviously from STAR LINK the blocks represent the union of the n subsystems which are equal to each other.
Having defined the architecture, we proceed with the realisation of the RBDs.
First of all, the failure rates of all subsystems are shown, with also the reliability value R, which is obtained using the following formula:

$$R = e^{-FR \cdot t} \tag{3.1}$$

Where with "FR" is indicated the Failure Ratio and with "t" the time in hour.

Id	Employed technology	Order of magnitude	Failure Rate	Reliability
R_A	Turboshaft	Power kW	$1{,}50{\cdot}10^{-5}$	0,999985
R_B	Gearbox	Gear ratio RPM	$5{,}26{\cdot}10^{-7}$	0,9999995
R_C	Wholly Superconducting Generator	Power kW	$2{,}54{\cdot}10^{-6}$	0,999997
R_D	Rectifer	Volt V	$1{,}84{\cdot}10^{-5}$	0,99998
R_E	AC Buses	Volt V	$1{\cdot}10^{-16}$	≈ 1
R_F	Superconducting Magnetic Energy Storage	Volt V	$7{,}61{\cdot}10^{-6}$	0,999992
R_G	Superconductiong Fault Current Limiter	Ampere A	$1{\cdot}10^{-16}$	≈ 1
R_H	SSCB (switches)		$1{\cdot}10^{-10}$	≈ 1
R_I	Inverter	Volt V	$7{,}06{\cdot}10^{-6}$	0,999993
R_L	Three-phase Superconducting Propulsor Motor	Power kW	$4{,}53{\cdot}10^{-6}$	0,999995
R_M	DC Buses	Volt V	$1{\cdot}10^{-16}$	≈ 1
R_{Pump}	Pump	Scope $\frac{m^3}{s}$	$1{,}49{\cdot}10^{-6}$	0,999998
R_{Tank}	Tank	Volume l	$8{,}65{\cdot}10^{-8}$	0,99999991

Table 3.1: ≪N3-X Subsystems/Components Reliability≫- 2023

The values in this table were obtained in general from:
The first RBD analysed is the logistics RBD. This aims to identify the reliability of the system and all its subsystems and components regardless of the various logical connections they have with each other. Consequently, the result that comes out is the most stringent one can have, since any failure means the loss of everything. In the light of the above, the logistical RBD is the putting together in series of all the blocks mentioned above, with even the propellant system with pumps and tanks.

Figure 3.3: ≪N3-X Logistic RBD≫- 2023

Having reached this point since the logistic RBD is being dealt with, the values in the table 3.1 are multiplied by each other considering the number of components.

$$R_{logistic} = R_A^2 \cdot R_B^2 \cdot R_C^4 \cdot R_D^4 \cdot R_E^{40} \cdot R_F^4 \cdot R_G^{134} \cdot R_H^{215} \cdot R_I^{16} \cdot R_L^{16} \cdot R_M^{56} \cdot R_{pump}^4 \cdot R_{tank}^4 \quad (3.2)$$

The final value of the entire system, reported as the failure rate, is $3.37 \cdot 10^{-4}$.
Considering the level of detail taken into consideration, especially for the mechanical components, it was decided to compare this RBD with that derived from a twin-engine aircraft with a Turbofan. For a Turbofan, the failure rate from the study [33] is $2{,}67 \cdot 10^{-6}$ and is derived by putting the two engines in series because the logistic

failure rate is $1.16 \cdot 10^{-5}$. Basically you have 1 order of magnitude separating the logistic RBDs of the N3-X with a generic twin-engine, but by today's standards this is not acceptable. On the other hand, one can imagine mitigating this value bearing in mind that most failure rates are derived by considering systems and elements that are currently being studied. Consequently, with the development of these technologies, better values of failure rates will occur and the RBD will tend to the value of turbofans or even something better. Logically, the success of these developments is closely linked not only with safety, but also with the cost of such investments. To summarise as things stand at present, N3-X is an aircraft that requires frequent maintenance, with the consequent increase in operating costs.
Having defined the logistic RBD, we proceed to the safety RBD:

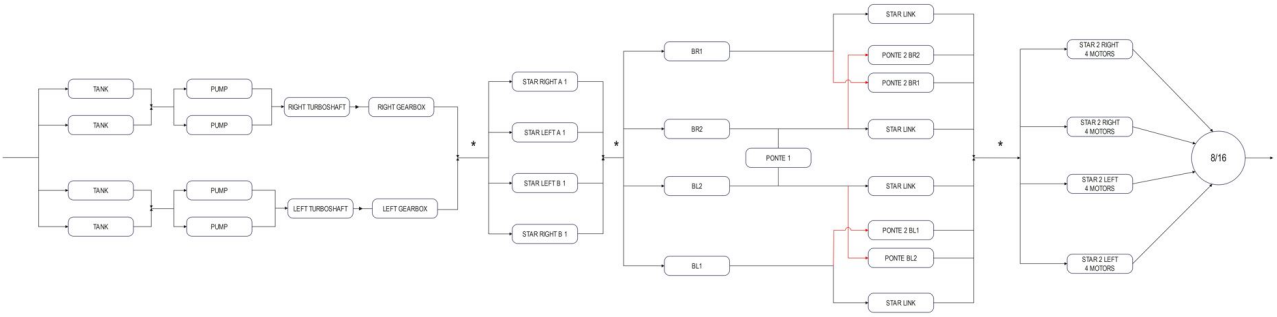

Figure 3.4: ≪N3-X Simplified Safety RBD≫ - 2023

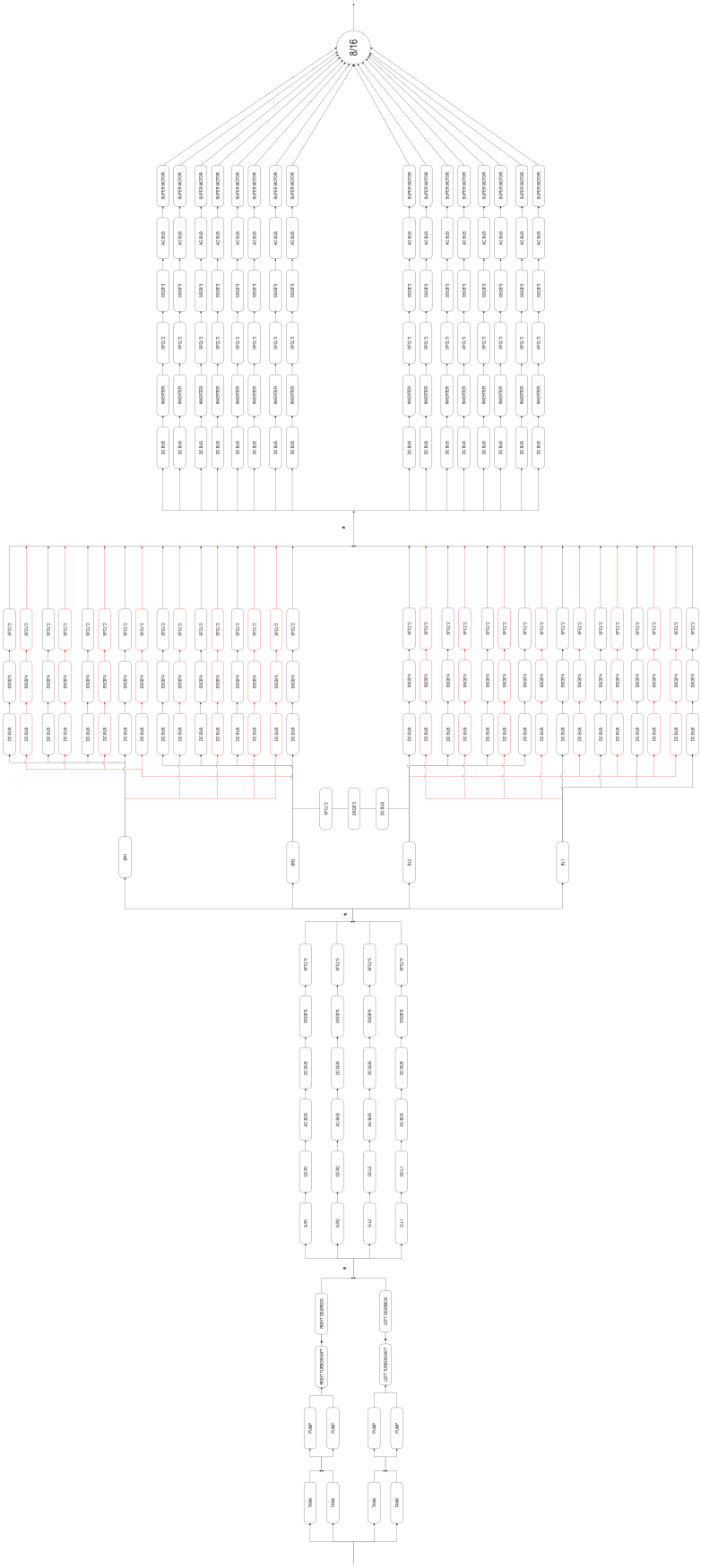

Figure 3.5: ≪N3-X Complete Safety RBD≫- 2023

These representations were arrived at based on the above statements, i.e. that 8 of the 16 engines must be running and that one of the 2 turboshafts must be operational. Therefore the 2 generators, with the power supply system in series, are in parallel with each other. but the respective gearboxes feeding the alternators must follow them in series, as their breakage would compromise the downstream line to the buses.
At this point we proceed with the first of four simplifications, namely that of closing the parallel. In order to be able to analyse the whole system clearly and effectively, it was decided to divide the RBD into four macro sections, in series with each other. The first macro section, the one described above, relates to endothermic engines, the second to the generation of energy and its storage, the third to the dissemination of that energy, and the last to electric propulsion.
Continuing with the second macro-section, based on the figure 3.4, we have the STAR 1, which are in parallel with each other since ultimately only one working bus of the 4 is needed for safety. These STAR 1s are different from those defined above, as they lack the energy storage and line bus. The reason for this lies in the fact that the accumulator is not designed to ensure full-electric flight, but only to compensate for any thrust requirements on the part of the pilots in the cruise phase; while the line bus has been carried over to the third macro-section.
At this point, we proceed with the analysis of the third section. In this one the line buses are opened in parallel, which are indicated in figure 3.4 with the following abbreviations: BR1, BR2, BL2 and BL1. Between BR2 and BL2 there is PONTE 1, which results in an "H" connection between the buses shown above and the STARLINKS and any downstream PONTE 2. This configuration was chosen because this subsystem is the only physical connection between the two arms, but its failure would not compromise the nominal work of the system. Continuing with the description, we have the STARLINK and PONTE 2. The latter are placed at an "S" to the STARLINK, and it should also be noted that these blocks in the image 3.5 indicate 4 connection lines, for a total of 32 lines.
Finally we have the STAR 2, which represent 4 of the final 16 lines.
These are placed in the "R" (r-out-of-n) configuration to ensure the condition of the 8 motors out of the 16 working. Obviously if we remain in the STAR 2 perspective, the output sees 2 of the 4 subsystems running.
Having said that, we proceed with the calculation of the above. For simplicity's sake, the overall formula is not shown, but only those relating to the various macro sections, since the overall formula is simply the product of the 4 results of the formulas shown. Proceeding in order, we have:

$$R_{S1} = 1 - (1 - R_A \cdot R_B \cdot (1 - (1 - R_{Tank})^2) \cdot (1 - (1 - R_{Pump})^2))^2 \tag{3.3}$$

The equation shown here represents the first subsection. In this you can see the parallel of the two propulsion arms with the values of the Turboshfts, Gearboxes and fuel systems in series. These consist for simplicity's sake of two interconnected tanks and two pumps, one for each tank. In reality, this system would be much more complex, but to get a reliable estimate of its reliability, it was deemed sufficient to reduce it to the tanks and pumps. Therefore, to estimate the reliability of the supply system, it was decided to put the parallels of the tanks and pumps in series.

$$R_{S2} = 1 - (1 - R_C \cdot R_H^9 \cdot R_G^5 \cdot R_M \cdot R_E \cdot R_D)^4 \tag{3.4}$$

In R_{S2} there is simply the parallel of the four lines from the generators to the line buses, not included.

$$\begin{aligned} R_{S3} = ((&R_M \cdot R_G^2 \cdot R_H^3) \cdot R_M^2 \cdot ((1 - (1 - R_M)^2) \cdot \\ &(1 - (1 - R_M \cdot R_G^2 \cdot R_H^4)^8 \cdot (R_M \cdot R_G^2 \cdot R_H^4)^8 + \\ &(1 - R_M)^2 \cdot (R_M \cdot R_G^2 \cdot R_H^4)^1 6)) + (1 - R_M \cdot R_G^2 \cdot R_H^3) \cdot \\ &(R_M^4 \cdot (1 - (1 - R_M \cdot R_G^2 \cdot R_H^4)^2)^{16} + R_M^3 \cdot (1 - R_M) \cdot \\ &(1 - (1 - R_M \cdot R_G^2 \cdot R_H^4)^2)^8 \cdot (R_M \cdot R_G^2 \cdot R_H^4)^8 + \\ &4 \cdot R_M^2 \cdot (1 - R_M)^2 \cdot (R_M \cdot R_G^2 \cdot R_H^4)^1 6) \end{aligned} \tag{3.5}$$

RS3 represents the power supply connections. The setting of the formula is based on whether or not PONTE 1 works. In the case that it does work, this means that there is a problem upstream of the line buses, so the cases where 3 and 2 line buses work, BR2 and BL2 respectively, and possibly one of the other two, have been given. At this point, the various cases of STARLINK and PONTE 2 block operation were considered. A similar procedure was carried out in the case that PONTE 1 did not work, considering 4, 3 and 2 buses working with or without STARLINK and PONTE 2.

$$
\begin{aligned}
R_{S4} = 1 - ((1 - R_M \cdot R_G^3 \cdot R_H^3 \cdot R_I \cdot R_E \cdot R_L)^{16} + \\
16 \cdot R_M \cdot R_G^3 \cdot R_H^3 \cdot R_I \cdot R_E \cdot R_L \cdot (1 - R_M \cdot R_G^3 \cdot R_H^3 \cdot R_I \cdot R_E \cdot R_L)^{15} \cdot \\
120 \cdot (R_M \cdot R_G^3 \cdot R_H^3 \cdot R_I \cdot R_E \cdot R_L)^2 \cdot (1 - R_M \cdot R_G^3 \cdot R_H^3 \cdot R_I \cdot R_E \cdot R_L)^{14} \cdot \\
560 \cdot (R_M \cdot R_G^3 \cdot R_H^3 \cdot R_I \cdot R_E \cdot R_L)^3 \cdot (1 - R_M \cdot R_G^3 \cdot R_H^3 \cdot R_I \cdot R_E \cdot R_L)^{13} \cdot \\
1820 \cdot (R_M \cdot R_G^3 \cdot R_H^3 \cdot R_I \cdot R_E \cdot R_L)^4 \cdot (1 - R_M \cdot R_G^3 \cdot R_H^3 \cdot R_I \cdot R_E \cdot R_L)^{12} \cdot \\
4368 \cdot (R_M \cdot R_G^3 \cdot R_H^3 \cdot R_I \cdot R_E \cdot R_L)^5 \cdot (1 - R_M \cdot R_G^3 \cdot R_H^3 \cdot R_I \cdot R_E \cdot R_L)^{11} \cdot \\
8008 \cdot (R_M \cdot R_G^3 \cdot R_H^3 \cdot R_I \cdot R_E \cdot R_L)^6 \cdot (1 - R_M \cdot R_G^3 \cdot R_H^3 \cdot R_I \cdot R_E \cdot R_L)^{10} \cdot \\
11440 \cdot (R_M \cdot R_G^3 \cdot R_H^3 \cdot R_I \cdot R_E \cdot R_L)^7 \cdot (1 - R_M \cdot R_G^3 \cdot R_H^3 \cdot R_I \cdot R_E \cdot R_L)^9 \cdot \\
12870 \cdot (R_M \cdot R_G^3 \cdot R_H^3 \cdot R_I \cdot R_E \cdot R_L)^8 \cdot (1 - R_M \cdot R_G^3 \cdot R_H^3 \cdot R_I \cdot R_E \cdot R_L)^8
\end{aligned}
\tag{3.6}
$$

This last formula represents the "R" diagram of electric motors and their power supply, in fact it can be seen that the products of the components are always repeated in the formula.
Finally, the product of these 4 formulas gives the value of the reliability of the entire system, which is given as the failure rate: $3.44 \cdot 10^{-9}$.
This value, considering the complexity of the entire system, the number of components and the current level of technology with which the failure rate values were derived, is in line with expectations. This does not mean that this value is sufficient, because compared to that of a current wight body aircraft, which is worth $7{,}13 \cdot 10^{-12}$ [33], there are at least 3 orders of magnitude of difference.
But if, instead of considering the value of the classical configuration reported earlier, one were to consider the value derived from the study [34], one would have the same order of magnitude as N3-X, but in the analysis to be conservative, this estimate would not be taken into account.
Consequently, what is reported at the safety level, not counting performance, this architecture would not be able to meet safety standards, but this does not detract from the fact that with the development of the technologies adopted, the scheme presented is sufficient.

Turning to the RBD of the flight phases, it can be seen that the following configurations are used to complete the mission:
For the take-off, climb and start of cruise phase, one can consider the logistic type RBD, i.e. all components in series. This is because in the initial phases of the mission, in the event of a failure, the entire mission would be aborted. Consequently, the value of this analysis is the same as that of the logistic RBD.

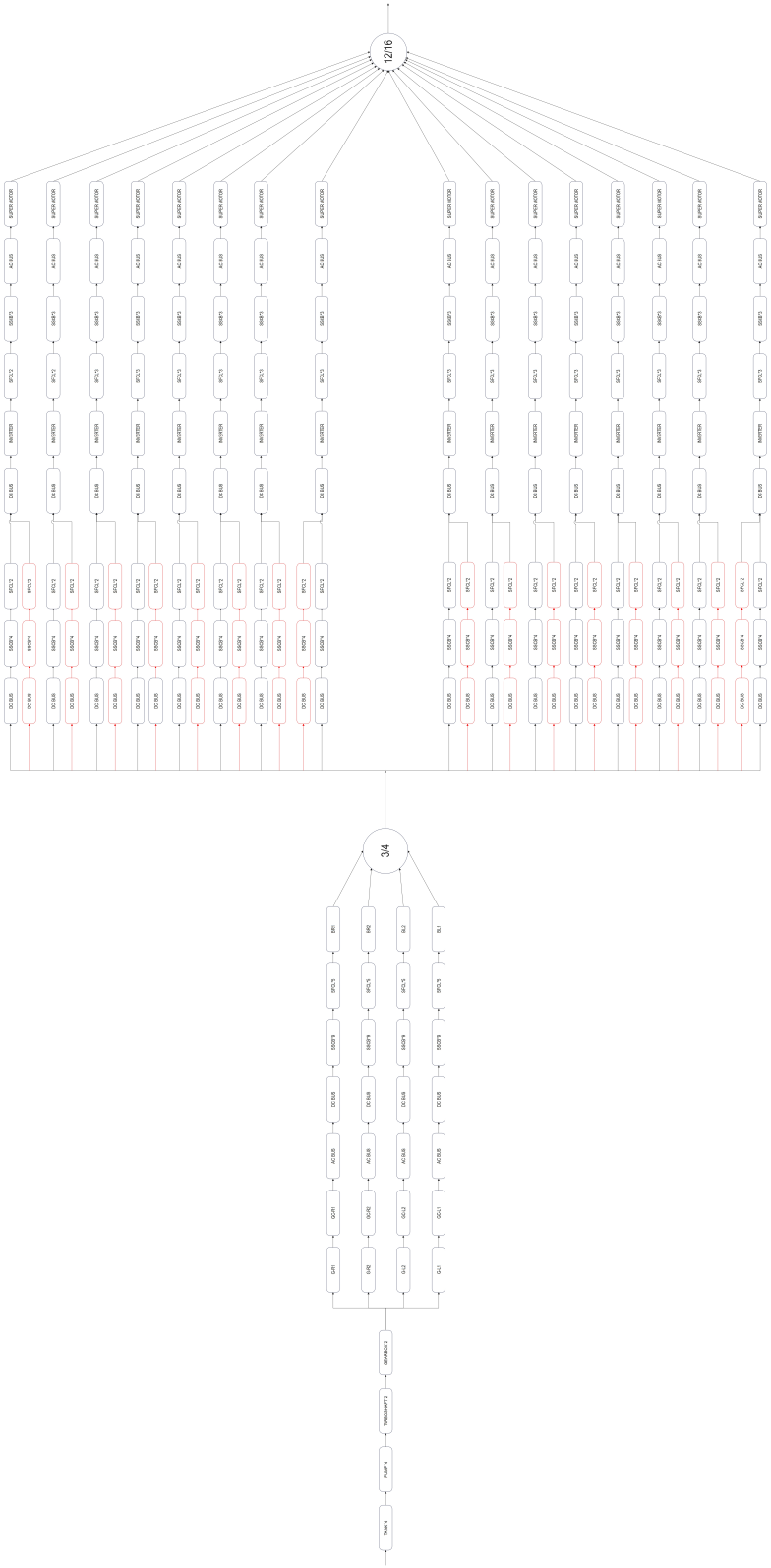

Figure 3.6: ≪N3-X Complete Cruise RBD≫ - 2023

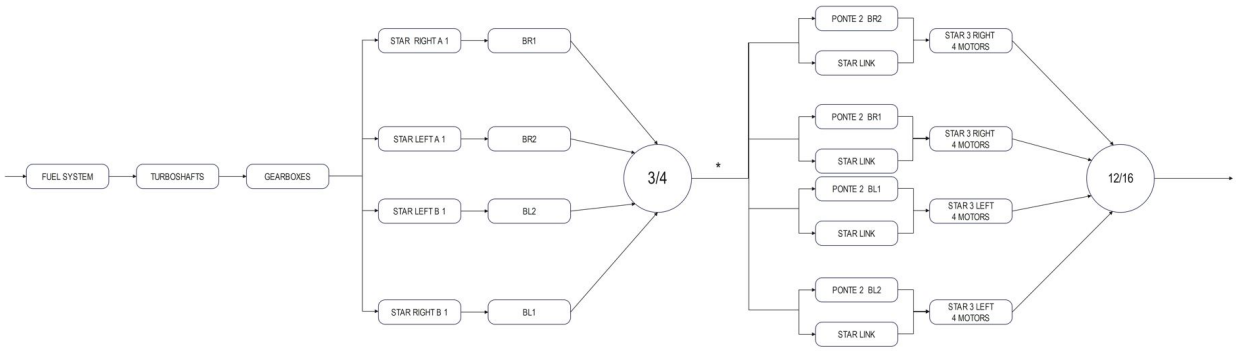

Figure 3.7: ≪N3-X Cruise RBD≫- 2023

Then in the cruise phase, the turboshafts, gearboxes and STAR 1s are placed in series, since the failure of one of these components generates a condition sufficient to abort the mission. Turning to the STAR 1s in series with the line buses and the energy accumulators, they are in the 'R' configuration because two out of four lines are sufficient to ensure cruise operation. This implies that the PONTE 1 could be disregarded because its operation is strictly related to emergency conditions and therefore to safety. Of course these configuration is simplified like the others in safety RBD. Finally, for what is downstream of STAR 1, it has been decided to maintain the "R" configuration of STAR 2 with the parallel of the STARLINK and PONTE 2 in series upstream, relative to the line.
To define the minimum number of working engines in the cruise phase, such that it is possible to complete the mission safely, the performance of the aircraft was analysed. Data from documents [32] and [35] were used to make this estimate.
Document [32] shows that the thrust power required by the aircraft during cruise is 10 MW, while the power required at take-off is 25 MW. From this it can be deduced that under nominal conditions the 16 engines must provide a maximum thrust of 1.5625 MW, while under safe conditions twice as much, i.e. 3.125 MW. The study also provides that in the event of one of the two generators failing, the engines must ensure a power output of 1.79 MW. This is followed by the determination of the thrust-to-weight ratio at the beginning of the mission and at the end. From the paper [35], it can be seen that the ratio is 0.183 at the start and 0.219 at the end. This implies that the power required in the final phases of the mission is less than that at the start, and from this we also deduce that the power required to have a go-around at the end of the mission is 20.89 MW, and this can be satisfied by a minimum number of 14 engines out of 16, if the maximum power for each individual engine is considered to be equal to that of the nominal conditions. If the maximum power for the case of a generator failure is considered, the minimum number of engines required to guarantee a reattachment drops to 12.
In the light of the above, the value of 12 motors was chosen for the study carried out in this thesis.

This is because it allows for more margin in the event that some electric motors break down, even if this means putting more strain on the surviving motors, but only in the event of a go-around. In fact, in the cruise phase, remember that the power required is 10 MW, so theoretically, if the engines always operated at 1.79 MW, 6 engines would be sufficient to guarantee flight.
We will now proceed with the calculation of the RBD and as was done for the safety RBD, it will be treated by breaking down the formula into macro sections in series with each other.

$$\begin{aligned} R_{C1} = 1 - ((1 - R_C \cdot R_H^9 \cdot R_G^5 \cdot R_M^2 \cdot R_E \cdot R_D \cdot R_F)^4 + \\ 4 \cdot R_C \cdot R_H^9 \cdot R_G^5 \cdot R_M^2 \cdot R_E \cdot R_D \cdot R_F \cdot (1 - R_C \cdot R_H^9 \cdot R_G^5 \cdot R_M^2 \cdot R_E \cdot R_D \cdot R_F)^3 + \\ 6 \cdot (R_C \cdot R_H^9 \cdot R_G^5 \cdot R_M^2 \cdot R_E \cdot R_D \cdot R_F)^2 \cdot (1 - R_C \cdot R_H^9 \cdot R_G^5 \cdot R_M^2 \cdot R_E \cdot R_D \cdot R_F)^2 \end{aligned} \tag{3.7}$$

R_{C1} represents what has been described above with the 'R' diagram of star 1 with line buses and accumulators.

$$\begin{aligned} R_{C2} = (R_M \cdot R_G^3 \cdot R_H^3 \cdot R_I \cdot R_E \cdot R_L \cdot (1 - (1 - R_M \cdot R_G^2 \cdot R_H^4)^2))^{16} + \\ 16 \cdot (R_M \cdot R_G^3 \cdot R_H^3 \cdot R_I \cdot R_E \cdot R_L \cdot (1 - (1 - R_M \cdot R_G^2 \cdot R_H^4)^2))^{15} \cdot \\ (1 - (R_M \cdot R_G^3 \cdot R_H^3 \cdot R_I \cdot R_E \cdot R_L \cdot (1 - (1 - R_M \cdot R_G^2 \cdot R_H^4)^2))) + \\ 120 \cdot (R_M \cdot R_G^3 \cdot R_H^3 \cdot R_I \cdot R_E \cdot R_L \cdot (1 - (1 - R_M \cdot R_G^2 \cdot R_H^4)^2))^1 4 \cdot \\ (1 - (R_M \cdot R_G^3 \cdot R_H^3 \cdot R_I \cdot R_E \cdot R_L \cdot (1 - (1 - R_M \cdot R_G^2 \cdot R_H^4)^2)))^2 + \\ 560 \cdot (R_M \cdot R_G^3 \cdot R_H^3 \cdot R_I \cdot R_E \cdot R_L \cdot (1 - (1 - R_M \cdot R_G^2 \cdot R_H^4)^2))^{13} \cdot \\ (1 - (R_M \cdot R_G^3 \cdot R_H^3 \cdot R_I \cdot R_E \cdot R_L \cdot (1 - (1 - R_M \cdot R_G^2 \cdot R_H^4)^2)))^3 + \\ 1820 \cdot (R_M \cdot R_G^3 \cdot R_H^3 \cdot R_I \cdot R_E \cdot R_L \cdot (1 - (1 - R_M \cdot R_G^2 \cdot R_H^4)^2))^{12} \cdot \\ (1 - (R_M \cdot R_G^3 \cdot R_H^3 \cdot R_I \cdot R_E \cdot R_L \cdot (1 - (1 - R_M \cdot R_G^2 \cdot R_H^4)^2)))^4 \end{aligned} \tag{3.8}$$

RC2 represents the final "R" diagram, where 12 of the 16 lines must operate. These lines, as mentioned before, have the STARLINKS and PONTE 2 in parallel with the STAR 2 components in series.
Then, putting together s s with the other components in series gives the following formula:

$$R_C = R_{Tank}^4 \cdot R_{Pump}^4 \cdot R_A^2 \cdot R_B^2 \cdot R_{C1} \cdot R_{C2} \tag{3.9}$$

This results in a failure rate of $3.74 \cdot 10^{-5}$, which is in line with the value for the traditional architecture, if not better, that has the same order of magnitude. Undoubtedly, the treatment of the cruise RBD deserves a more in-depth discussion considering in which phase of the cruise the aircraft finds itself. But to a first approximation, the analysis performed is considered more than sufficient.

Finally, for the descent and landing phase, with eventual reattachment, the scheme made for safety is considered sufficient, with the only difference being that the electric motors required are not 8 but 12.
This follows from what has been described for the cruise phase.

3.2 SUGAR VOLT

For the SUGAR Volt, the discussion is based on the document [12], where the 2.12 architecture is discussed in the previous chapter. It only reiterates that the electrical subsystems operate in the turbofan only on the low-pressure shaft, so that only the fan and the first stages of the compressor are powered. This leads to the RBDs.
First, the values of the failure rates of the various components are given, and they are:

Id	Employed technology	Order of magnitude	Failure Rate	Reliability
R_A	Turbofan	Thrust N	$2{,}67{\cdot}10^{-6}$	0,999997
R_B	Batteries Block	Volt V	$9{,}31{\cdot}10^{-6}$	0,9999907
R_C	Electric Motor	Power kW	$4{,}53{\cdot}10^{-6}$	0,999995
R_D	Inverter	Volt V	$7{,}06{\cdot}10^{-6}$	0,999993
R_E	AC Buses	Volt V	$1{\cdot}10^{-16}$	≈ 1
R_F	DC Buses	Volt V	$1{\cdot}10^{-16}$	≈ 1
R_{Pump}	Pump	Scope $\frac{m^3}{s}$	$1{,}49{\cdot}10^{-6}$	0,999998
R_{Tank}	Tank	Volume l	$8{,}65{\cdot}10^{-8}$	0,99999991

Table 3.2: ≪SUGAR VOLT Subsystems/Components Reliability≫- 2023

For the logistic RBD, we have the same treatment analysed in the previous paragraph (where it will no longer be restated from now on) and we have that the failure rate is $5.34 \cdot 10^{-5}$. Compared to its predecessor, this architecture is only slightly better, and is more in line with that of the traditional two turbofan system, which

is worth $1.16 \cdot 10^{-5}$ [33]; moreover, it should be remembered that this value will improve with the development of the various subsystems/components.

Moving on to analyse the security-related RBD:

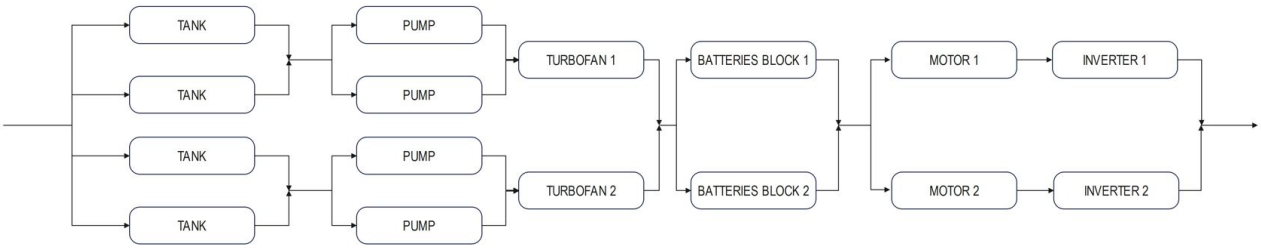

Figure 3.8: ≪SUGAR VOLT Safety RBD≫ - 2023

To be able to define safety RBD, it is necessary to go into more detail about how this technology works. In fact, as far as a Turbofan is concerned, the electric motor powered by the battery operates in what is called the 'low-pressure shaft'. In this shaft are the fan and part of the compressor and axial turbine. This shaft is called the low-pressure shaft because in the compressor there is the first increase in pressure relative to the external environment. Then between the low-pressure compressor and the low-pressure turbine is the 'high-pressure shaft', where the axial high-pressure compressor and turbine are located. Between these two is the combustor, and everything is well described by the figure below:
Moving on to analyse the security-related RBD:

At this point, it is easy to see the image of the safety RBD. To ensure that thrust is generated, it is necessary for either the electrical part or the chemical part to work. Therefore, the idea was to put the thermal part in series with the batteries and the electrical component. However, each block sees the various sub-systems in parallel: for the thermal part you have the two turbofans in parallel, for the batteries you see their two packs, i.e. the left and right motor packs, and for the electrical part you see the motors and inverters in parallel (which are in series with each other).
Having made this consideration, it is necessary to talk about the degree of hybridisation. This indicates how the energy supplied to generate thrust is divided up. In the case of the SUGAR Volt project, three degrees of hybridisation were analysed: the Balanced 1380 Hp with an electrical energy fraction of 12.2%, the Balanced 1750 Hp with an electrical fraction of 13.4% and the Core Shutdown 7150 Hp with an electrical fraction of 32.7% [29].
Having defined this, one can understand the choice of safety RBD. In fact, based on current regulations, which say that in the event of a failure of one of the two propulsion units, the surviving one must be able to provide the missing thrust and

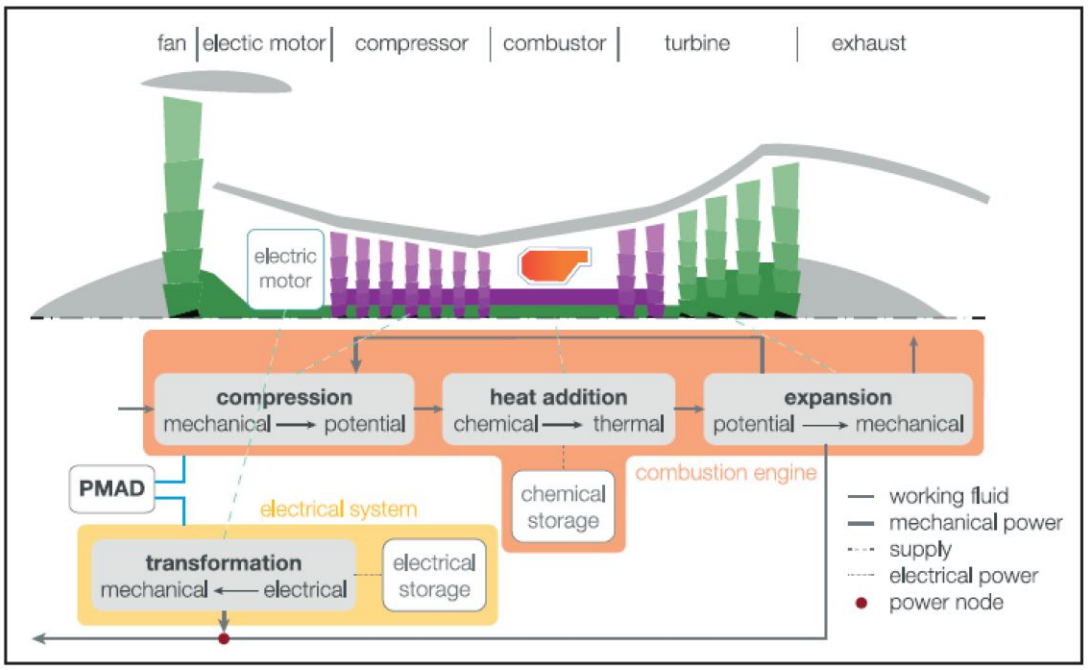

Figure 3.9: ≪Turbofan engine scheme with electric-assisted propulsion≫- Performance analysis of an electrically assisted propulsion system for a short-range civil aircraft - 2019

it is necessary to ensure that one of the two turbofans and one of the two inverter and motor blocks must be operational. But since a failure of the turbofan does not necessarily compromise the related electrical part, it was decided to use a partitioned redundancy or 'H' scheme RBD that is always functional.
Having said this, we proceed with the reliability calculation using the following formula:

$$RBD_{Safety} = (1-(1-R_A \cdot (1-(1-R_{Tank})^2) \cdot (1-(1-R_{Pump})^2))^2) \cdot \\ (1-(1-R_B)^2) \cdot (1-(1-R_C R_D) \cdot (1-R_C R_D)) \cdot R_E \cdot R_F \tag{3.10}$$

As a result we have a faliure rate of $2.28 \cdot 10^{-10}$, which is a better value compared to N3-X, plus it is closer with current aviation standards. Of course, as with the logistic RBD, when there is an improvement in the technology used, this value will improve to bring the system up to current values.
Finally, we proceed to discuss the RBDs for the flight phases.
In the take-off and climb phase, RBD is equal to the logistic one, which means all subsystems are in series with each other. Whereas in the cruise phase, under nominal conditions, thrust is given only by the contribution of the two turbofans. This allows two hypotheses to be made: either only the thermal engines are considered, without considering the electrical part, or both parts are considered. This reasoning

is a child of the degree of hybridisation, since the electric part does not have a sufficient contribution to provide a minimum of useful thrust to keep the aircraft in the air, it could be disregarded.

Figure 3.10: ≪SUGAR VOLT Cruise RBD≫- 2023

Since it is necessary for the electrical part to be functional in the descent and landing phase, it is also necessary for it to be functional in the cruise phase (even if it is not used). Consequently, the RBD for cruise is like the logistic RBD.
This choice was made because for SUGAR the degree of hybridisation is around 10/30% and this does not allow for more articulated RBDs as in the case of having a hybridisation around 50%, which means that the electric and thermal parts are equivalent.
Finally, for the descent and landing phase, since the mission is almost over, it is possible to consider the RBDs equivalent to the one presented for safety.

3.3 X-57 MAXWELL

For the Maxwell, the study that is carried out is based on the paper [12], where the following architecture is given:

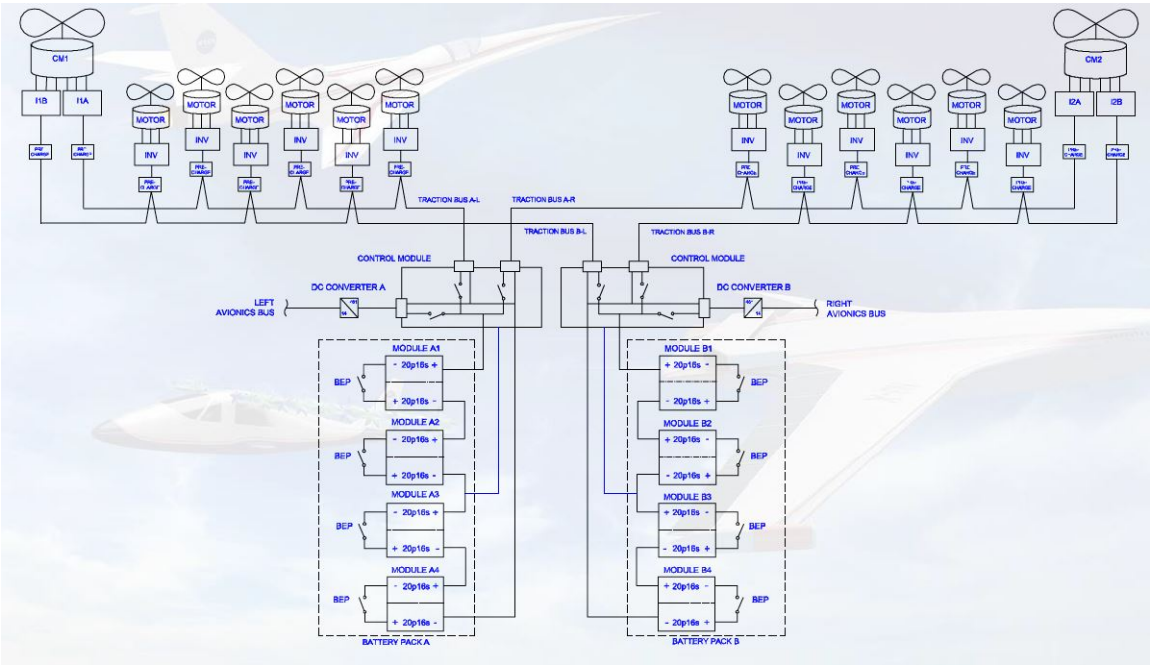

Figure 3.11: "X-57 Maxwell Control Concept of Operations"- SCEPTOR Power System Desi-gn:Experimental Electric Propulsion System Design and Qualification for Crewed Flight Testing -2016

This is a full electric aircraft, where batteries/fuel cells provide the energy for the various engines. The architecture depicted here is the 'Mod IV' design stage, i.e. the final one.
We now proceed to define the various failure rates of the subsystems:

Id	Employed technology	Order of magnitude	Failure Rate	Reliability
R_A	Batteries block	Volt V	$9{,}31{\cdot}10^{-6}$	0,9999907
R_B	Control Modules		$2{,}79{\cdot}10^{-5}$	0,99997
R_C	AC/DC Buses	Volt V	$1{\cdot}10^{-16}$	≈ 1
R_D	Motor Controllers		$4{,}75{\cdot}10^{-6}$	0,999995
R_E	Three-phase Electric Motors	Power kW	$4{,}53{\cdot}10^{-6}$	0,9999995
R_F	Cruise Motors	Power kW	$4{,}53{\cdot}10^{-6}$	0,999995
R_G	Take-off Motors	Power kW	$9{,}24{\cdot}10^{-6}$	0,9999907
R_H	Inverter	Volt V	$7{,}06{\cdot}10^{-6}$	0,999993

Table 3.3: ≪X-57 MAXWELL Subsystems/Components Reliability≫- 2023

As usual, the logistic one sees the various components put in series and results in $3.44 \cdot 10^{-4}$.
This value is even slightly better than the reference propulsion unit, the pistonprop. In fact, its value is $6{,}32 \cdot 10^{-4}$ [36]. Moreover, as with previous architectures, technological development will improve this estimate even more than the reference one. Moving on to safety, a consideration must be made with regard to the aircraft's overall architecture. The designers, in order to make the wings and the propulsion system more efficient, decided on a configuration with two cruise engines at the wing

tip and 12 thrust engines distributed over the two wings. This choice has brought several benefits, such as reducing the wing surface area by more than 50% and improving the lift coefficient Cp, but it also has several criticalities. Among these is the safety study.
Indeed, with the current state of the design, it is not possible to determine a well-defined RBD like other architectures. The fact that the cruise engines are positioned at the end of the wings does not make it possible to state that in the event of a One Engine Inoperative (OEI)[1], the aircraft is capable of counteracting the yawing moment given by the surviving engine, even if the 6 thrust engines of the wing of the failed cruise engine are in operation. For this reason, it was decided to operate two RBDs, where one considers that the thrust motors opposite the surviving engine are capable of counteracting the yawing moment, while the other is not.
Consequently, the latter can be considered the more conservative.
Below are the RBDs:

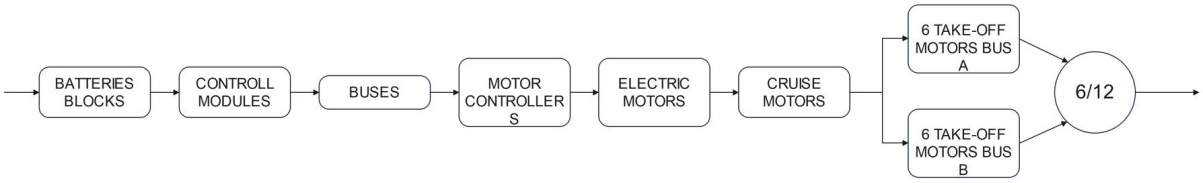

Figure 3.12: ≪X-57 MAXWELL Security RBD vr.1≫- 2023

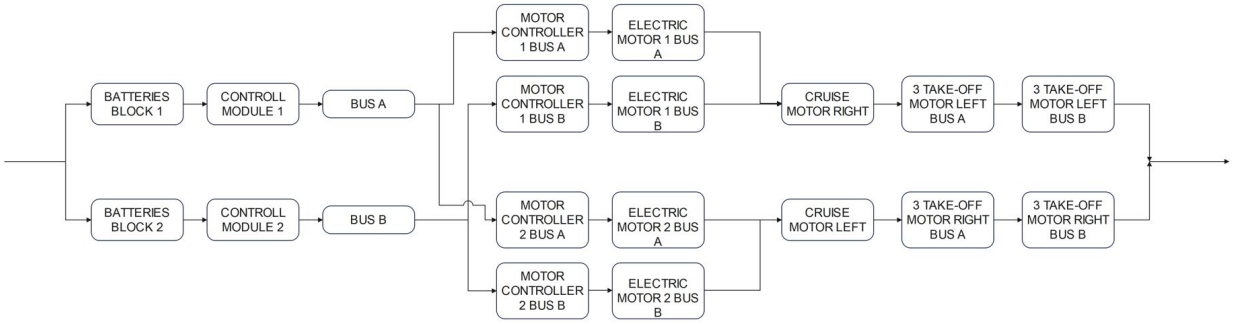

Figure 3.13: ≪X-57 MAXWELL Security RBD vr.2≫- 2023

The first RBD is the most conservative. The various blocks represent the components of the same family grouped together in series. The thrust engines must guarantee the functionality of at least 6 out of 12 engines.
The second RBD represents, on the other hand, the case where when you have OEI you can fly using the thrust motors as well. In general, one can see a scheme with

[1]OEI means only in the event that one of the cruise engines should fail.

two series in parallel linked by a double 'S'.
Going into detail, we can see that the first three blocks in parallel on the left represent the power supply, then going to the right we have the cruise motors which are powered from both sides of the power supply. Finally, there are the thrust motors in series with respect to the cruise motors.
The reason for their arrangement in series in the parallel arm stems from the consideration of the analysis [37] where the engine powers at take-off are indicated. In fact, the cruise engines provide a power of 80 kW, while the thrust engines 13 kW. So when there is an OEI, the thrust engines on a wing can provide almost equal power to that of the missing engine.
Naturally, the powers indicated on the analysis [37] are the nominal ones, which in the event of an emergency will certainly be much higher. Consequently, it is possible to assume that in the event of an OEI in the take-off phase, in order to guarantee the flight envelope, the surviving cruise motor and the thrust motors of the opposite wing are kept active, while the thrust motors of the surviving cruise wing must be deactivated.
We now proceed to calculate the reliability of the two RBDs; the formulae derived from the diagrams are presented below:

$$\begin{aligned} R_{Reliability_1} = {} & (1-(1-R_A R_B R_C)^2) R_D^4 R_E^4 R_F^2 R_H^4 \\ & (1-(((1-R_H R_I)^{12}) + (11 R_H R_I (1-R_H R_I)^{11}) + (10(R_H R_I)^2 (1-R_H R_I)^{10}) \\ & + (9(R_H R_I)^3 (1-R_H R_I)^9) + (8(R_H R_I)^4 (1-R_H R_I)^8) + (7(R_H R_I)^5 (1-R_H R_I)^7) \\ & + (6(R_H R_I)^6 (1-R_H R_I)^6))) \end{aligned} \tag{3.11}$$

$$\begin{aligned} R_{Reliability_2} = {} & 2(R_A R_B R_C R_F R_H^3 R_I^3) - (R_A R_B R_C)^2 (R_F R_H^3 R_I^3)^2 \\ & + (2 R_D R_E R_I (R_A R_B R_C R_F R_H^3 R_I^3 + (R_A R_B R_C)^2 (R_F R_H^3 R_I^3)^2 \\ & - (R_A R_B R_C)^2 R_F R_H^3 R_I^3 - (R_F R_H^3 R_I^3)^2 R_A R_B R_C)) \end{aligned} \tag{3.12}$$

The first formula represents the most conservative case and its value is $7.44 \cdot 10^{-5}$. Even this is a little unacceptable compared to a pistonprop architecture with two engines, that is $9{,}79 \cdot 10^{-8}$. Whereas the value resulting from the second formula is $4{,}23 \cdot 10^{-9}$.
The latter is far better than the original aircraft. But it must be remembered that this does not take into account the possibility of yawing moment contrast, which

is the discriminating factor in choosing one RBD over the other.In general, in the light of the above, this architecture is in line, albeit slightly worse, with that of a pistonprop architecture.
We now proceed with RBD of the flight phases.
For the take-off and climb phase we have logistic RBD, whereby all components must be functional.
For the cruise phase the matter becomes more complicated, because nominally only the two cruise engines are operational and the thrust engines have their propellers folded to reduce aerodynamic drag.
As a result, two RBDs have been defined, one where the cruise engines must absolutely work, so you have all the blocks in series and this is related to the fact that in the case of OEI the aircraft cannot counteract the yawing moment given by the surviving engine, even if the thrust engines were used. While the second sees precisely the case in which the thrust engines manage to counter this yawing moment. To summarise, in the first case we have an RBD with all components in series, and in the second an RBD as the safety one. But since the thrust engines are not designed to operate for the cruise phase, and also considering the particular nature of the aircraft, it was decided to use only the RBD with all subsystems in series.
Finally, moving on to the descent and landing phases, the RBD with all components in series is also maintained.

3.4 DRAGON ONERA

For the DRAGON ONERA, the study is based on the paper [14]. Its is a distributed turbo-electric architecture, very similar to NASA's N3-X, the only difference being that the DRAGON does not have accumulators 2.6.
Consequently, given the similarity, you also have RBDs and components that are similar to each other:

Id	Employed technology	Order of magnitude	Failure Rate	Reliability
R_A	Turboshaft	Power kW	$1{,}50{\cdot}10^{-5}$	0,999985
R_B	Gearboxes	Gear ratio RPM	$5{,}26{\cdot}10^{-7}$	0,99999995
R_C	Fault Current Limiters	Ampere A	$1{\cdot}^{-16}$	≈ 1
R_D	Generators	Power kW	$2{,}54{\cdot}10^{-6}$	0,999997
R_E	AC Buses	Volt V	$1{\cdot}10^{-16}$	≈ 1
R_F	Breakers	Ampere A	$1{\cdot}10^{-16}$	≈ 1
R_G	Inverters	Volt V	$7{,}06{\cdot}10^{-6}$	0,999993
R_H	Three-phase Electric Motors	Power kW	$4{,}53{\cdot}^{-6}$	0,999995
R_I	Rectifers	Volt V	$1{,}84{\cdot}10^{-5}$	0,99998
R_L	DC Buses	Volt V	$1{\cdot}10^{-16}$	≈ 1
R_{Pump}	Pump	Scope $\frac{m^3}{s}$	$1{,}49{\cdot}10^{-6}$	0,9999998
R_{Tank}	Tank	Volume V	$8{,}65{\cdot}10^{-8}$	0,999999991

Table 3.4: ≪DRAGON Subsystems/Components Reliability≫- 2023

The logistic RBD sees all components in series and has a value of $5.86 \cdot 10^{-4}$.

$$R_{Logistic} = R_{Tank}^4 \cdot R_{Pump}^4 \cdot R_A^2 \cdot R_B^4 \cdot R_D^4 \cdot R_C^{12} \cdot R_E^4 \cdot R_F^{24} \cdot R_L^{20} \cdot R_I^4 \cdot (R_L \cdot R_F^3 \cdot R_G \cdot R_E \cdot R_H \cdot)^{40} \tag{3.13}$$

This value when compared to both current aircraft and N3-X brings it in line with the values obtained. As with N3-X, this value will improve with the development of the technologies used.
We now proceed to the analysis of the safety RBD:

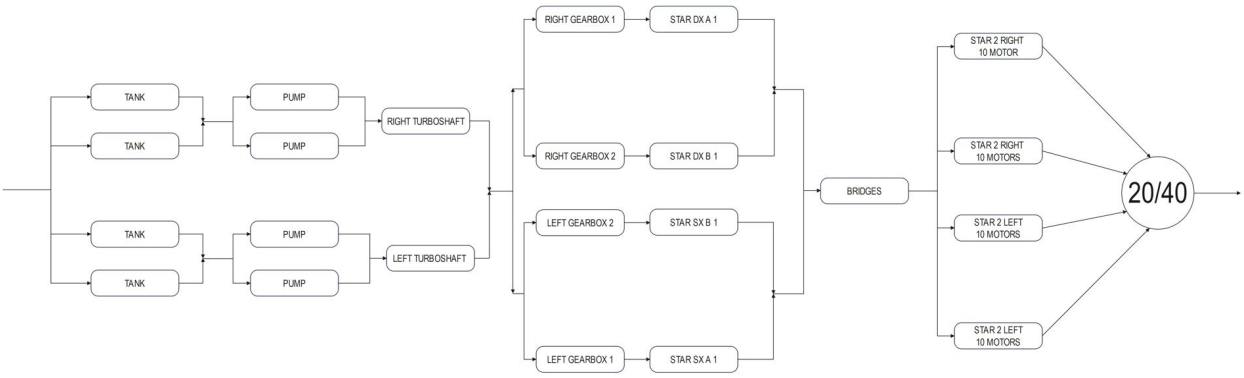

Figure 3.14: ≪DRAGON Simplified Safety RBD≫- 2023

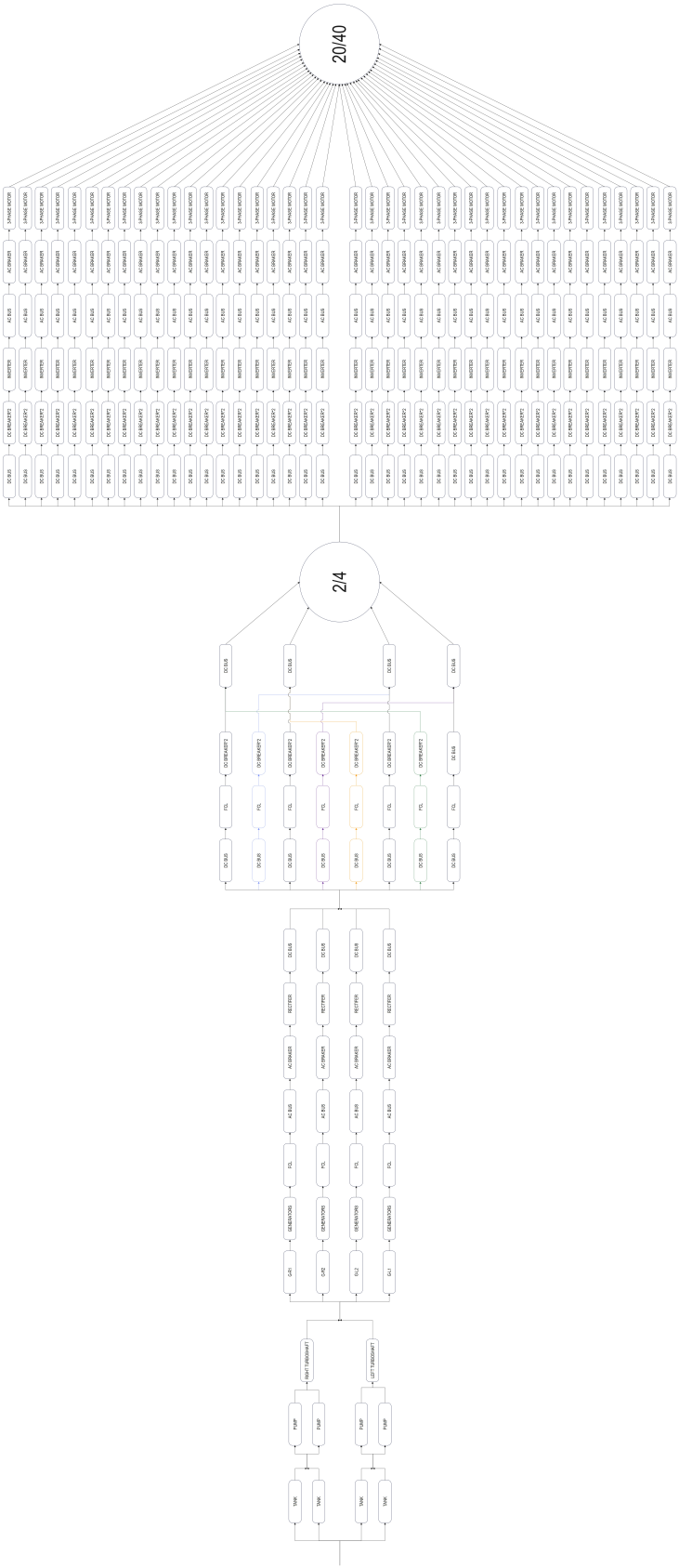

Figure 3.15: ≪DRAGON Complete Safety RBD≫ - 2023

Similar to N3-X, the safety requirements see the operation of at least 20 of the 40 electric motors and at least one of the two Turboshaft motors for power generation. Consequently, in this case too, the study was divided into macro sections.
The first two macro sections are very similar in architecture to those studied in the N3-X section, with the only difference being the gearboxes. In fact, in this case there are 4 gearboxes, so instead of being considered in the first section, they have been positioned upstream of the STAR 1. This results in having the Turboshaft units in parallel with the gearboxes in series with the STAR 1.
As can be seen from the figure 3.15, the lines of the STAR 1s consist of an AC generator with an AC bus downstream equipped with Fault Current Limiters and an AC breaker; then there is a current rectifier and the first DC bus. It should be remembered from the previous chapter that this architecture has no energy accumulators.
Proceeding with the third macro section, based on the image 3.14, we have the connections between the first DC line buses (which for simplification have been considered in the second macro section) with the second DC line buses, which go directly to supply the thruster lines (macro section 4).
The architecture of these connections sees that two power lines depart from the first DC line bus. One goes to the second DC bus of the reference line, i.e. the one that works nominally, while the second one goes as redundancy to another DC bus of the line.In order we have that the second DC buses in relation to the 4 first DC buses have the following connections: 1:4, 2:3, 3:1 and 4:2. In practice the first bus can receive current from both the first DC bus and the fourth, the second from the second and the third, the third from the third and the first, and finally the last from the fourth and the second. These connections consist of a DC bus, a Fault Current Limiter and two DC Breakers.
The last macro section sees the 40 power supply lines placed in an 'R' configuration to ensure the operation of at least 20 out of 40 motors. These lines in turn consist of a DC bus, two DC breakers, an inverter, a C bus with an AC breaker, and finally the three-phase electric motor.
As already done for N3-X, we now proceed with the calculation of the failure rate by first calculating the reliability of the 4 macro sections and then their product.
For the first macro section we have:

$$R_{S1} = 1 - (1 - R_A \cdot (1 - (1 - R_{Tank})^2) \cdot (1 - (1 - R_{Pump})^2))^2 \tag{3.14}$$

This equation, as mentioned earlier, is practically the same as the one seen in N3-X with the only difference being that the gearboxes are missing. The next equation representing the second macro section is also the same as N3-X:

$$R_{S2} = 1 - (1 - R_B \cdot R_D \cdot R_C \cdot R_E \cdot R_F \cdot R_G \cdot R_L)^4 \tag{3.15}$$

$$\begin{aligned}
R_{S3} = {} & ((R_L \cdot R_C \cdot R_F^2)^4 + (R_L \cdot R_C \cdot R_F^2)^4 \cdot (1 - R_L \cdot R_C \cdot R_F^2) + \\
& (R_L \cdot R_C \cdot R_F^2)^3 \cdot (1 - R_L \cdot R_C \cdot R_F^2)^2 + (R_L \cdot R_C \cdot R_F^2)^4 \cdot (1 - R_L \cdot R_C \cdot R_F^2)^2 + \\
& (R_L \cdot R_C \cdot R_F^2)^3 \cdot (1 - R_L \cdot R_C \cdot R_F^2)^3 + (R_L \cdot R_C \cdot R_F^2)^2 \cdot (1 - R_L \cdot R_C \cdot R_F^2)^4 + \\
& (R_L \cdot R_C \cdot R_F^2)^4 \cdot (1 - R_L \cdot R_C \cdot R_F^2)^3 + (R_L \cdot R_C \cdot R_F^2)^3 \cdot (1 - R_L \cdot R_C \cdot R_F^2)^4 + \\
& (R_L \cdot R_C \cdot R_F^2)^2 \cdot (1 - R_L \cdot R_C \cdot R_F^2)^5 + (R_L \cdot R_C \cdot R_F^2)^4 \cdot (1 - R_L \cdot R_C \cdot R_F^2)^4 + \\
& (R_L \cdot R_C \cdot R_F^2)^3 \cdot (1 - R_L \cdot R_C \cdot R_F^2)^5 + (R_L \cdot R_C \cdot R_F^2)^2 \cdot (1 - R_L \cdot R_C \cdot R_F^2)^6) \cdot \\
& R_L^4 + ((R_L \cdot R_C \cdot R_F^2)^3 + (R_L \cdot R_C \cdot R_F^2)^3 \cdot (1 - R_L \cdot R_C \cdot R_F^2) + \\
& (R_L \cdot R_C \cdot R_F^2)^2 \cdot (1 - R_L \cdot R_C \cdot R_F^2)^2 + (R_L \cdot R_C \cdot R_F^2)^2 \cdot (1 - R_L \cdot R_C \cdot R_F^2)) \cdot \\
& R_L^3 \cdot (1 - R_L) + ((R_L \cdot R_C \cdot R_F^2)^2 + (R_L \cdot R_C \cdot R_F^2)^2 \cdot (1 - R_L \cdot R_C \cdot R_F^2)) \cdot \\
& R_L (1 - R_L)^2
\end{aligned} \tag{3.16}$$

This equation was derived by considering the various cases of operation of the various connections, depending on the operation of the downstream line bus. Thus, there are many combinations when all buses are operating, while there are only 2 when only 2 buses are operating. At the very least, two line buses must always operate to ensure the supply of at least 20 motors.
These combinations were chosen over the 'R' scheme because the lines upstream of the line buses, due to the architecture, cannot be considered in parallel. These lines, if you want to trace them back to a scheme, are like an "S" scheme intertwined between the two rows of line buses. Consequently, the approach described earlier was chosen.
In addition, it can be seen from the equation that there is no distinction between the nominal links and the redundancies, since on a constitutive level they are the same. From this statement, it can be understood when only nominal lines are considered and when redundant lines are in operation or not.
To underline the concept, we proceed with three examples taken from the equation. At the beginning are the first values all raised to the fourth, these represent the nominal case. The second group, to the right of the first, always presents the operation of 4 lines, but one of these is a redundancy, in fact this value is followed by the product with the non-operation of the nominal line. Finally, always following the direction of the equation, one can see the case where only 3 nominal lines operate, with the failure of both the nominal line and its redundancy.

We now proceed to the last macro section:

$$
\begin{aligned}
R_{S4} = {} & (R_L \cdot R_F^3 \cdot R_G \cdot R_E \cdot R_H)^{40} + 40 \cdot (R_L \cdot R_F^3 \cdot R_G \cdot R_E \cdot R_H)^{39} \cdot \\
& (1 - R_L \cdot R_F^3 \cdot R_G \cdot R_E \cdot R_H) + 780 \cdot (R_L \cdot R_F^3 \cdot R_G \cdot R_E \cdot R_H)^{38} \cdot \\
& (1 - R_L \cdot R_F^3 \cdot R_G \cdot R_E \cdot R_H)^2 + 9880 \cdot (R_L \cdot R_F^3 \cdot R_G \cdot R_E \cdot R_H)^{37} \cdot \\
& (1 - R_L \cdot R_F^3 \cdot R_G \cdot R_E \cdot R_H)^3 + 91390 \cdot (R_L \cdot R_F^3 \cdot R_G \cdot R_E \cdot R_H)^{36} \cdot \\
& (1 - R_L \cdot R_F^3 \cdot R_G \cdot R_E \cdot R_H)^4 + 658008 \cdot (R_L \cdot R_F^3 \cdot R_G \cdot R_E \cdot R_H)^{35} \cdot \\
& (1 - R_L \cdot R_F^3 \cdot R_G \cdot R_E \cdot R_H)^5 + 3838380 \cdot (R_L \cdot R_F^3 \cdot R_G \cdot R_E \cdot R_H)^{34} \cdot \\
& (1 - R_L \cdot R_F^3 \cdot R_G \cdot R_E \cdot R_H)^6 + 18643560 \cdot (R_L \cdot R_F^3 \cdot R_G \cdot R_E \cdot R_H)^{33} \cdot \\
& (1 - R_L \cdot R_F^3 \cdot R_G \cdot R_E \cdot R_H)^7 + 76904685 \cdot (R_L \cdot R_F^3 \cdot R_G \cdot R_E \cdot R_H)^{32} \cdot \\
& (1 - R_L \cdot R_F^3 \cdot R_G \cdot R_E \cdot R_H)^8 + 273438880 \cdot (R_L \cdot R_F^3 \cdot R_G \cdot R_E \cdot R_H)^{31} \cdot \\
& (1 - R_L \cdot R_F^3 \cdot R_G \cdot R_E \cdot R_H)^9 + 847660528 \cdot (R_L \cdot R_F^3 \cdot R_G \cdot R_E \cdot R_H)^{30} \cdot \\
& (1 - R_L \cdot R_F^3 \cdot R_G \cdot R_E \cdot R_H) 10 + * * *
\end{aligned}
\tag{3.17}
$$

The equation should proceed until we have 20 engines running out of 40, but numerically this is not necessary since the terms in that range have an infinitesimal weight compared to the final result. Consequently, it was decided to stop with the calculation at the tenth iteration, which for convenience coincides with 30 out of 40 working engines, a necessary condition for cruising.
Finally, by taking the product of the four equations, we obtain that the failure rate is $2.25 \cdot 10^{-10}$. Again, it is a good value, but to compareed to the conventional one, which we remember is $7{,}13 \cdot 10^{-12}$ [33], it is non right. Naturally, as in N3-X, the technological development of the various sub-systems/components will increase their reliability, despite the large number of elements that architectures have.

Having defined the safety RBD, we proceeded with the study of the flight phases.
For take-off and ascent, it was decided to use the logistic RBD, although as far as what was the fourth macro section of the safety RBD was concerned, it is conceivable that the loss of a few lines (no more than 10) might not compromise the mission. But this statement must possibly be verified by future studies.
Turning to the cruise RBD, we have the following RBD:

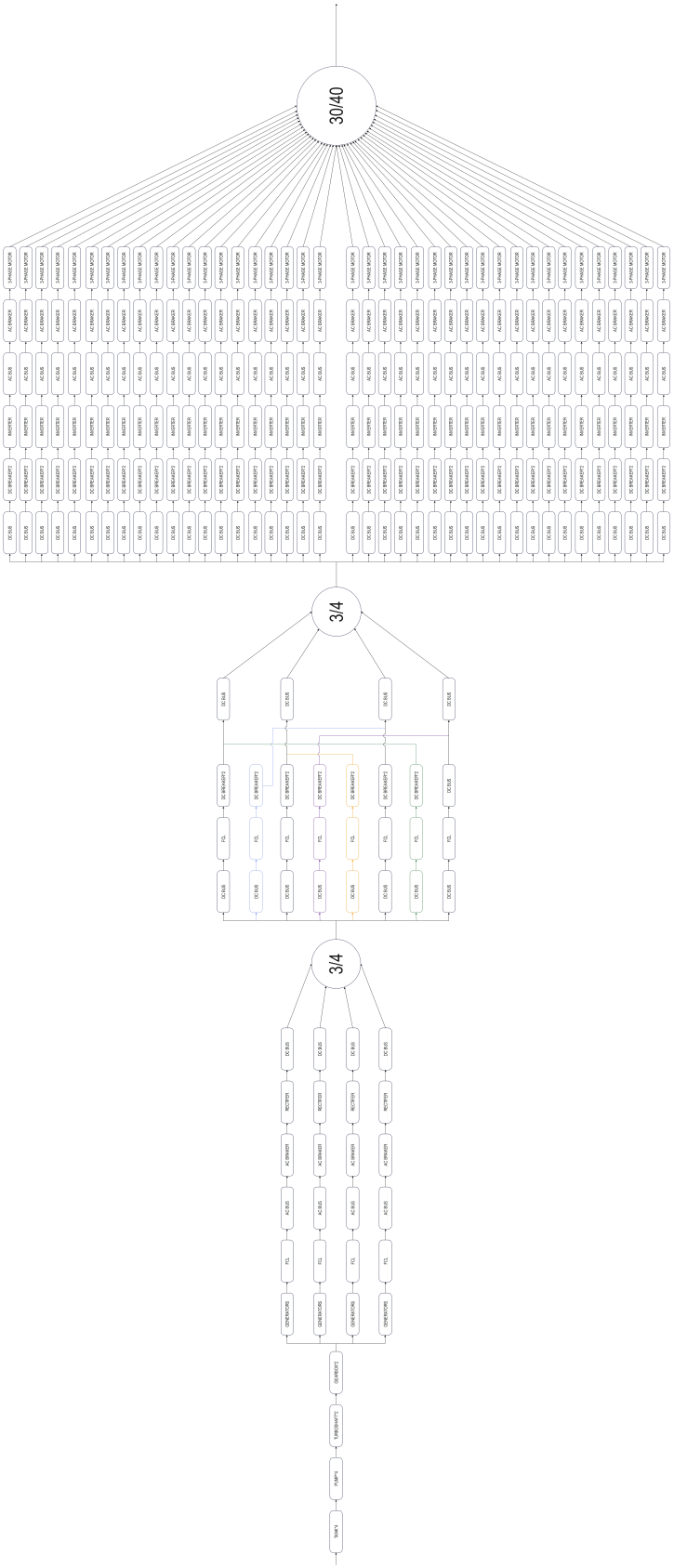

Figure 3.16: «DRAGON Complete Cruise RBD»- 2023

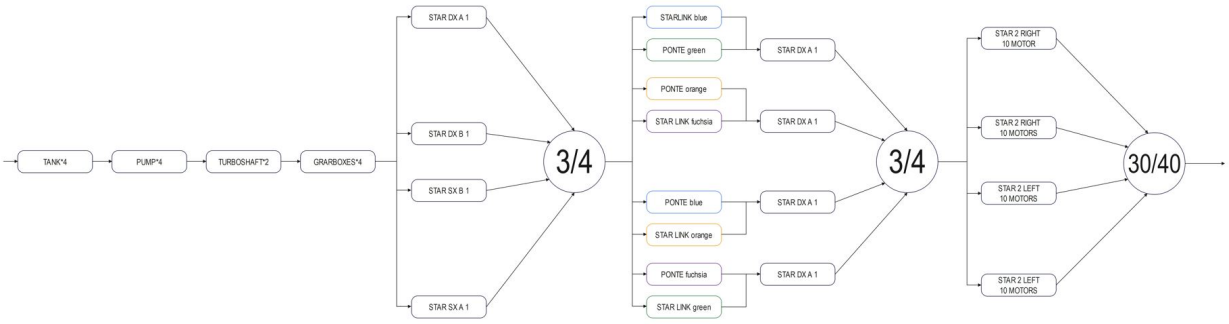

Figure 3.17: ≪DRAGON Cruise RBD≫- 2023

Basically, the simplification made for the safety one is repeated. The first macro section has all the components of the endothermic system and the gearboxes in series. Then STAR 1 has an "R" diagram with 3 out of 4 working lines. Similarly, the third macro section sees that 3 out of 4 of the second DC bus lines must work, with upstream connections. Finally, the fourth macro section is the same as the fourth safety section, but must ensure at least 30 out of 40 lines.
We now proceed to calculate the reliability of the second, third and fourth macro sections and then the total reliability:

$$\begin{aligned} R_{C2} = &(R_D \cdot R_C \cdot R_E \cdot R_F \cdot R_G \cdot R_L)^4 + \\ &4 \cdot (R_D \cdot R_C \cdot R_E \cdot R_F \cdot R_G \cdot R_L)^3 \cdot (1 - R_D \cdot R_C \cdot R_E \cdot R_F \cdot R_G \cdot R_L) \end{aligned} \tag{3.18}$$

$$\begin{aligned} R_{C3} = &((R_L \cdot R_C \cdot R_F^2)^4 + (R_L \cdot R_C \cdot R_F^2)^4 \cdot (1 - R_L \cdot R_C \cdot R_F^2) + \\ &(R_L \cdot R_C \cdot R_F^2)^3 \cdot (1 - R_L \cdot R_C \cdot R_F^2)^2 + (R_L \cdot R_C \cdot R_F^2)^4 \cdot (1 - R_L \cdot R_C \cdot R_F^2)^2 + \\ &(R_L \cdot R_C \cdot R_F^2)^3 \cdot (1 - R_L \cdot R_C \cdot R_F^2)^3 + R_L \cdot R_C \cdot R_F^2)^4 \cdot (1 - R_L \cdot R_C \cdot R_F^2)^3 + \\ &((R_L \cdot R_C \cdot R_F^2)^3 \cdot (1 - R_L \cdot R_C \cdot R_F^2)^4 + (R_L \cdot R_C \cdot R_F^2)^4 \cdot (1 - R_L \cdot R_C \cdot R_F^2)^4 + \\ &(R_L \cdot R_C \cdot R_F^2)^3 \cdot (1 - R_L \cdot R_C \cdot R_F^2)^5) \cdot R_L^4 + \\ &((R_L \cdot R_C \cdot R_F^2)^3 + (R_L \cdot R_C \cdot R_F^2)^3 \cdot (1 - R_L \cdot R_C \cdot R_F^2)) \cdot \\ &R_L^3 \cdot (1 - R_L) \end{aligned} \tag{3.19}$$

It can be seen that R_{C3} is equal to R_{S3} minus the terms for two-bus operation. Finally, for R_{C4}, the formula 3.17 already used for safety.
This results in the following overall equation:

$$R_C = R_{Tank}^4 \cdot R_{Pump}^4 \cdot R_A^2 \cdot R_B^4 \cdot R_{C2} \cdot R_{C3} \cdot R_{C4} \tag{3.20}$$

The failure rate is equal to $5.86 \cdot 10^{-6}$, this result is better than today's standards and N3-X value. Moreover, the technological development of the implemented components will lead to better results than current architectures.
Finally, for the descent and landing phases, it was decided to maintain the cruise pattern.

3.5 STARC-ABL

For the STARC-ABL, the study is based on the document [12]. Its particular architecture makes it a special case study. In fact, since electric propulsion is only used in the cruise phase, whereas for the other phases of flight there is propulsion with two traditional turbofans, in terms of safety it is only necessary to consider the two endothermic engines, which, it should be remembered, have a value of $7{,}13 \cdot 10^{-12}$.
For the propulsion architecture, the reasoning is based on the image 2.7.
We now proceed with the RBDs. First, the table of component failure rates is defined:

Id	Employed technology	Order of magnitude	Failure Rate	Reliability
R_A	Turbofan	Thrust N	$2{,}67{\cdot}10^{-6}$	0,999997
R_B	Gearboxes	Gear ratio RPM	$5{,}26{\cdot}10^{-7}$	0,9999995
R_C	Rectifers	Volt V	$1{,}84{\cdot}10^{-5}$	0,99998
R_D	AC Buses	Volt V	$1{\cdot}10^{-16}$	≈ 1
R_E	Inverters	Volt V	$7{,}06{\cdot}10^{-6}$	0,999993
R_F	Three-phase Electric motors	Power kW	$4{,}53{\cdot}10^{-6}$	0,999995
R_G	Freewheels	Gear ratio RPM	$6{,}09{\cdot}10^{-6}$	0,999994
R_H	Propulsor	Thrust N	$6{,}04{\cdot}10^{-6}$	0,999994
R_I	Generators	Power kW	$2{,}54{\cdot}10^{-6}$	0,999997
R_J	DC Buses	Volt V	$1{\cdot}10^{-16}$	≈ 1
R_{Tank}	Tank	Volume l	$8{,}65{\cdot}10^{-8}$	0,99999991
R_{Pump}	Pump	Scope $\frac{m^3}{s}$	$1{,}49{\cdot}10^{-6}$	0,999998

Table 3.5: ≪STARC-ABL Subsystems/Components Reliability≫- 2023

At the logistic level, we have all components/systems in series and find a value of $1.32 \cdot 10^{-4}$.This value is also in line with the traditional one, although slightly worse. In fact, the slight deterioration comes mainly from the fact that more components are used and consequently more breakage can occur.
Moving on with the calculations, we proceed with the study of the flight phases,

where for take-off and climb we have an RBD equal to the logistic one. Whereas for the cruise RBD we have the following configuration:

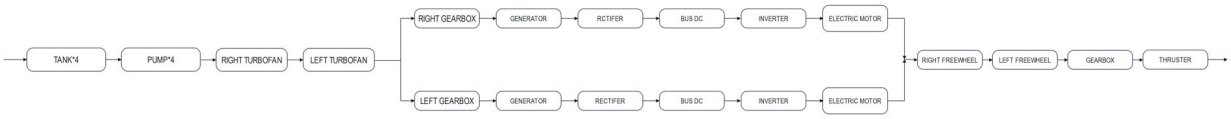

Figure 3.18: ≪STARC-ABL Cruise RBD≫- 2023

You consider the two turbofans in series, then from the gearboxes of the turbofans to the electric motors, you have a parallel configuration. This is because at the level of operability one can be less stringent, given the fact that one can switch from the turbo-electric configuration to the traditional one, so in the event one of the arms fails, one could continue with the mission. Whereas from the freewhell to the tail thruster, the series configuration was decided upon as the mission would degrade.
We proceed with the reliability calculation and have the following formula:

$$R_{Cruise} = R_{Tank}^4 \cdot R_{Pump}^4 \cdot R_A^2 \cdot (1 - (1 - R_B \cdot R_C \cdot R_D^2 \cdot R_E \cdot R_F \cdot R_I \cdot R_J)^2 \cdot R_G^8 \cdot R_B \cdot R_H \tag{3.21}$$

The result converted to failure rate is $6.70 \cdot 10^{-}5$. This result is also in line with today's standards, although in this case the technological developments of the components will have less of an effect than in the other architectures examined, because this study involves the use of current technologies and not their developments. Moreover, in the event of a loss of the electrical part, the aircraft can also fly with Turbofans alone. Because the amount of propellant is certainly calibrated to the use of the engines as power generators and not as thrust generators, this translates to lower fuel consumption and thus a possible sizing of the tanks so that they contain the bare minimum. Only further analysis on this issue can define the possible switch from turbo-electric to conventional architecture.
As already mentioned, it was decided not to deal with the safety RBD because the architecture of this aircraft allows it to fly in a traditional configuration, with the two turbofans acting as thrusters and not generators. Consequently, the safety RBD only sees the two Turbofans, with the fuel system in series, in parallel, which is the current standard.
Having defined this as the aircraft meeting safety standards, the values of the cruise and logistic RBDs, even if they are not too high, can already be considered sufficient

at the current level of technology. Of course with the development of such technologies, these values will be better and more in line with current standards.
Finally, for the descent and landing with reattachment, it is sufficient to consider the two turbofans in series without considering the turbo-electric part.

3.6 PEGASUS NASA

Finally, for PEGASUS, the study is based on the paper [12]. Like the STARC, it too has a peculiar architecture, in fact it can be considered a hybrid between the SUGAR and the MAXWELL.
The reference architecture is the one presented in 2.13, where we can see the presence of two Turboprop thrusters hybridised at the wing tip, plus three electric motors whose function is to provide extra thrust in the take-off and ascent phases. These are placed one pair in the inner part of the wings and the other in the tail of the aircraft. In essence, the PEGASUS is a parallel hybrid turbo aircraft with auxiliary electric motors.
We now proceed to determine the RBD. First, the failure rate table is given:

Id	**Employed technology**	**Order of magnitude**	**Failure Rate**	**Reliability**
R_A	Batteries Pack	Volt V	$9{,}31{\cdot}10^{-6}$	0,9999907
R_B	Turboprop from PW 127E	Power kW	$1{,}50{\cdot}10^{-5}$	0,999985
R_C	Inverters	Volt V	$7{,}06{\cdot}10^{-6}$	0,999993
R_D	Three-phase Electric Motor	Power kW	$4{,}53{\cdot}10^{-6}$	0,999995
R_E	Propeller Turbine	Power kW	$1{,}13{\cdot}10^{-5}$	0,999989
R_F	AC Buses	Volt V	$1{\cdot}10^{-16}$	≈ 1
R_G	DC Buses	Volt V	$1{\cdot}10^{-16}$	≈ 1
R_{Tank}	Tank	Volume V	$8{,}65{\cdot}10^{-8}$	0,99999991
R_{Pump}	Pump	Scope $\frac{m^3}{s}$	$1{,}49{\cdot}10^{-6}$	0,999998

Table 3.6: ≪PEGASUS NASA Subsystems/Components Reliability≫ - 2023

As is customary for the logistical RBD, all subsystems are taken in series. Its value is $1.35 \cdot 10^{-4}$. Which is worse by today's standards, even if only slightly, in fact the turboprop, having as its value that indicated on the table 3.6 leads to a failure rate of the conventional system of $3{,}63 \cdot 10^{-5}$. Naturally, as for the other architectures analysed, with the technological development of the components, a further improvement in the failure rate of the Pegasus could be achieved.
For the safety RBD, we have the following configuration:

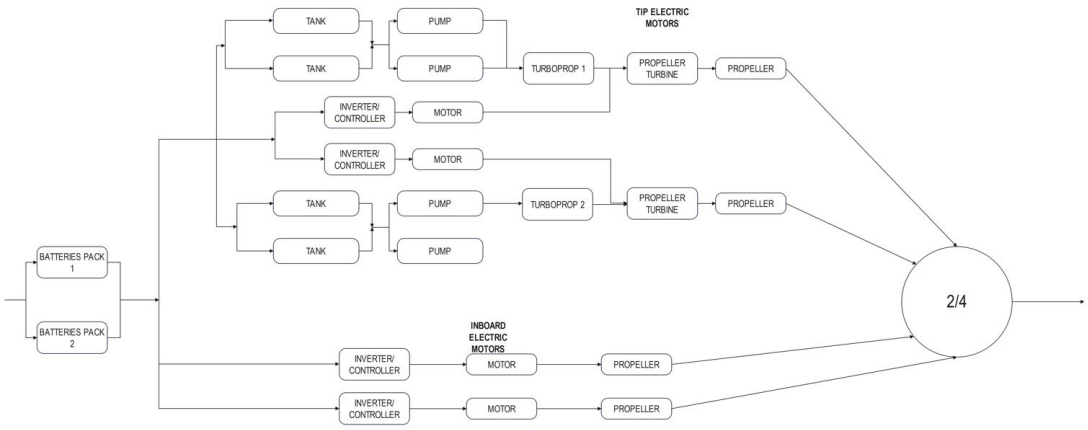

Figure 3.19: ≪PEGASUS Safety RBD≫- 2023

Starting from the left, we have the two battery packs in parallel. These are placed in series with the motors as they are critical components of the system.
Following this, we have the four propulsion units, which, based on what is stated in documents [30] and [38], are placed in parallel with each other. It should be emphasised that the electric motor at the rear is not considered, because the amount of thrust it provides, compared to other hybrid and full electric motors, is much less [30]. This is shown in the graph below:

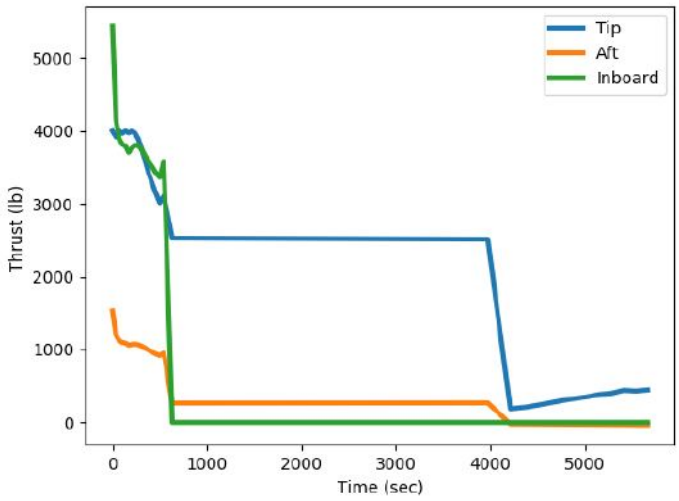

Figure 3.20: ≪Mission Thrust Profile≫- Analysis of the Parallel Electric-Gas Architecture with Synergistic Utilization Scheme (PEGASUS) Concept - 2019

Analysing the individual propulsion units we have the Turboprop Hybrid macro-group, where they are positioned at the wing tips. We have chosen to make an RBD with a doubly parallel configuration, because we must consider that these endothermic engines have the possibility of many degrees of hybridisation, linked to the fact of the nature of the thruster itself, which at the very least has two distinct shafts: one dedicated to the compressor and one dedicated to the propeller, where

the electric motor also operates. Document [8] analyses hybridised thrusters at 20%, while document [9] considers three degrees of hybridisation: 25%, 50% and 75%. In general, these hybrid engines can always generate thrust even if the endothermic component stops working[2].
Moving on to the electric motors, we have the block of inboard motors that are in parallel with each other. At this point we have the 'R' diagram between these electric motors and the hybrid ones. This is because, based on document [8], the aircraft must have batteries that allow it to fly in hybrid mode up to 400 nm (741 km) and in full electric mode up to 200 nm (370.5 km). Consequently, given the possibility of flying in both hybrid and electric modes, it is necessary that at least 2 out of 4 engines are running. Naturally, given the arrangement of the motors, it is necessary that they are not on the same wing, since in that case it is not necessarily possible to counteract the yawing moment with the aerodynamic surfaces alone.
Having defined this, we proceed with the reliability calculation:

$$\begin{aligned} R_{Reliability} = {} & (1-(1-R_A)^2)\cdot R_G\cdot(1-(((1-R_E\cdot(1-(1-R_B\cdot(1-(1-R_{Tank})^2)\cdot \\ & (1-(1-R_{Pump})^2))(1-R_C\cdot R_D\cdot R_F)))^2\cdot(1-R_C\cdot R_D\cdot R_F)^2)+ \\ & 2\cdot(1-(R_E)(1-(1-R_B\cdot(1-(1-R_B\cdot(1-(1-R_{Tank})^2)\cdot(1-(1-R_{Pump})^2))\cdot \\ & (1-R_C\cdot R_D\cdot R_F)))\cdot(1-(1-R_E\cdot(1-(1-R_B\cdot(1-(1-R_B\cdot(1-(1-R_{Tank})^2)\cdot \\ & (1-(1-R_{Pump})^2))\cdot(1-R_C\cdot R_D\cdot R_F))))\cdot(1-(1-R_C\cdot R_D\cdot R_F))^2+ \\ & 2\cdot(1-R_C\cdot R_D\cdot R_F)\cdot(1-(1-R_E\cdot(1-(1-R_B\cdot(1-(1-R_B\cdot(1-(1-R_{Tank})^2)\cdot \\ & (1-(1-R_{Pump})^2))\cdot(1-R_C\cdot R_D\cdot R_F))))^2\cdot(1-(1-R_C\cdot R_D\cdot R_F)) \end{aligned} \tag{3.22}$$

The result is $8.67\cdot10^{-11}$, which considering the complexity of the architecture is better than expected, in fact the value for the conventional turboprop system is $2.25\cdot10^{-10}$, a good one order of magnitude lower. If this value were to be confirmed, it would bode very well. Of course, more in-depth studies are needed to verify this claim.
Proceeding to the flight phases we have that for take-off and climb all systems must be in series with each other as in logistic RBD. For cruise RBD one has a situation similar to that of the MAXWELL project, where only the cruise engines are active and the electric motors are not used. In reality, one has that the tail electric motor is always in operation. In the light of this and what was said before, there are 3 RBDs

[2]Obviously, if the failure remains confined to the high-pressure shaft, which means that it does not also mechanically affect the shaft that drives the propeller.

for cruising: the first case sees only the endothermic motors being in series with each other, without considering the electric part, and this is possible when there are low degrees of hybridisation such as 20/25%, which with this electric component cannot compensate for the yawing moment given by the surviving motor. The value you get is $3.63 \cdot 10^{-5}$, in line with current standards.
The second case is when the degree of hybridisation is 50% and you have:

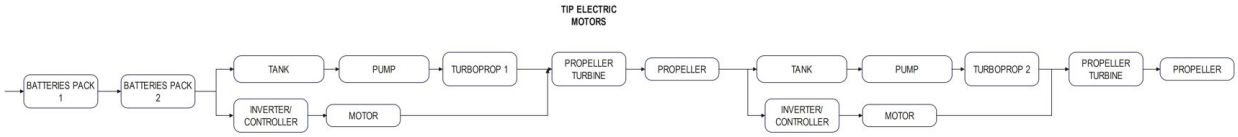

Figure 3.21: ≪PEGASUS Cruise RBD≫- 2023

As the picture shows, it can be seen that the electrical and endothermic components are in parallel with each other. Consequently, we have the following formula:

$$R_{Reliability} = R_A^2 \cdot (1 - R_E + (1 - (1 - R_B \cdot R_{Tank}^2 \cdot R_{Pump}^2)) \cdot (1 - R_C \cdot R_D \cdot R_F)))^2 \tag{3.23}$$

The result is $4.12 \cdot 10^{-5}$,which is better than the current technology by an order of magnitude. Of course, this value, like that for safety, needs to be verified, but it can be said that with the current level of technology it ensures the reliability required for the cruise phase with a 50% hybridisation.
Finally, there is the third case in which the degree of hybridisation is 75% and is like the first case described, with the difference that the electric part is used instead of the endothermic part. Its result is $6.44 \cdot 10^{-5}$, which is slightly worse than the previous analysis, but still better than the reference value.
For descent and landing, one has an RBD that reviews all components placed in series.

Chapter 4

NPRD Quaternion data interpretation

4.1 NPRD study

The estimation of failure rates used in the previous chapter is mainly based on the use of Quaternion's NPRD databook. Naturally, where there was an opportunity to use data from studies relevant to the various architectures discussed, it was chosen to use the latter, because most of these technologies are either in the research phase or, if they are used at all, are not used in the aviation sector or have other functions. Consequently, an initial attempt was made to find the relative data of the various failure rates from studies concerning the architectures under consideration. But in general, with the exception of the X-57 MAXWELL, failure rate data was either scarce or completely absent.
Consequently, to make up for this shortcoming, it was decided to proceed using values derived by analogy from today's technologies and to do this, the aforementioned NPRD (Nonelectronic Parts Reliability Data) from Quaternion solutions incorporated was used. This application contains data on the number of failures and the number of hours used of a variety of mechanical, electrical, electromechanical and assembly components, actually used by machinery derived not only from the aviation industry but also from others such as the naval or space industry. What has been done is to interpret these values so that they are as true as possible.
The version used is the 2016 version and was used for all components, with the exception of technologies such as turbofan, turboshaft, turboprop and pistonprop, which base their values on current regulations, and for some components of the MAXWELL, where data from article [39] was used, because the studies of this architecture are at a more advanced stage than the others and consequently it already has more in-depth reliability studies.
The application in general works that by going to the fault-finding page (in addition to this there are other different functions in the application) you have the following

view:

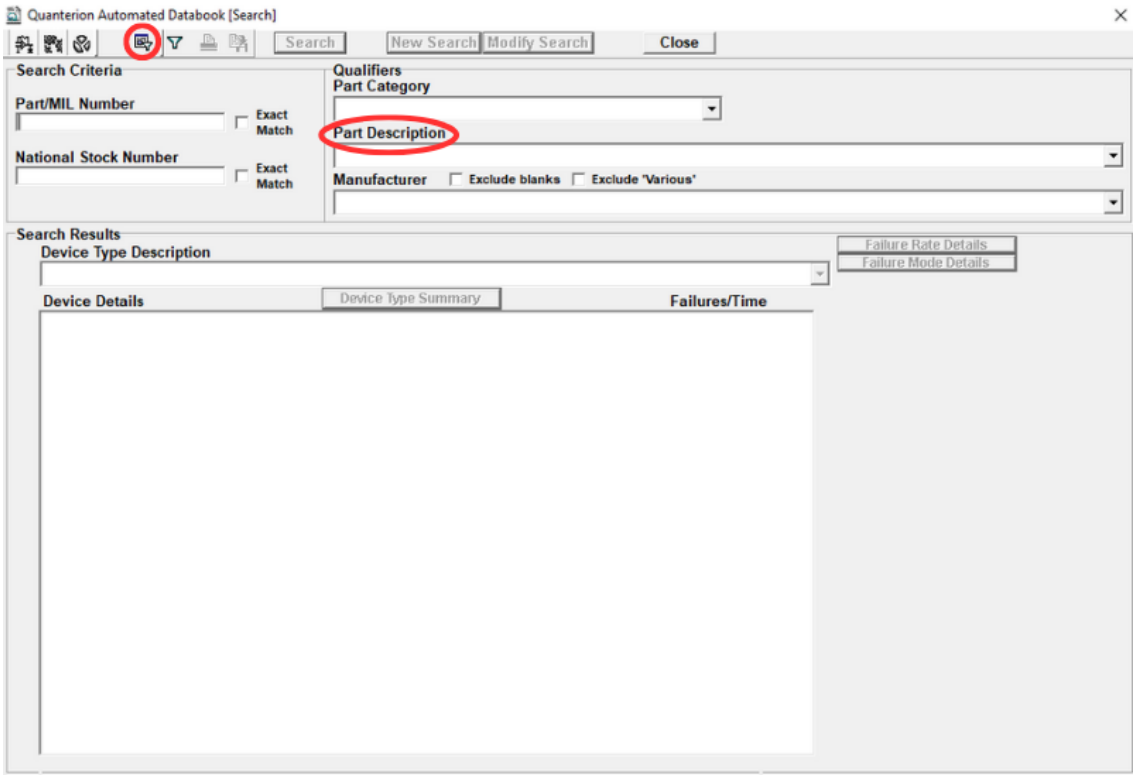

Figure 4.1: NPRD window

On this page, the elements we are interested in are the filters and the part description bar. To select filters, click in the red circle in the top left-hand c orner. This opens the window shown in the figure below:

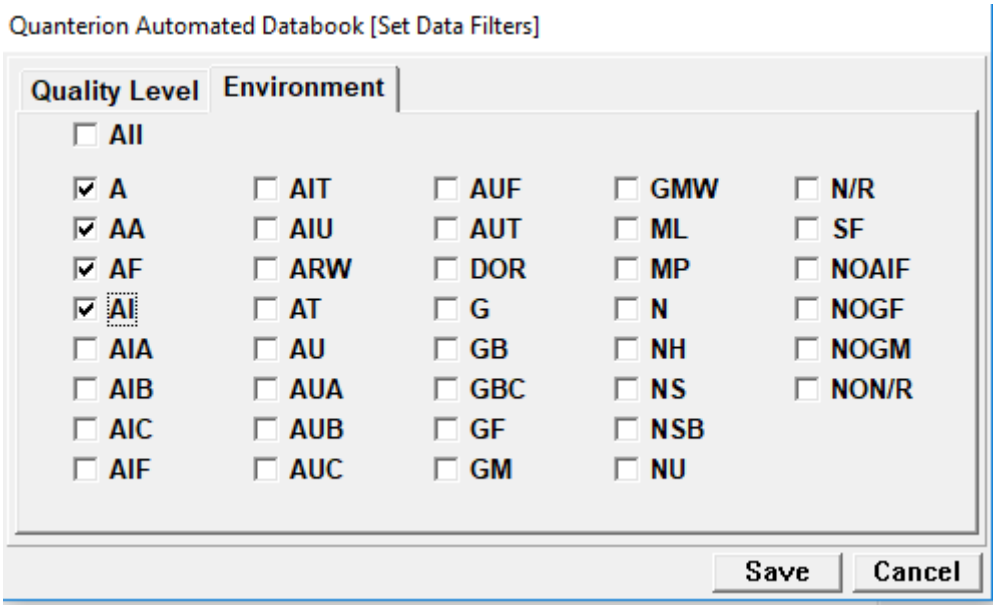

Figure 4.2: NPRD filtre page

Filters are necessary to select the components used in aeronautics, so that any extraneous elements are not considered. This does not mean that they have always been used, in fact especially for electrical components values without filters have been considered, this is because one must always bear in mind that the architectures under consideration have no counterparts in reality. As a result, it is true that they exploit existing technologies or any developments thereof, but these technologies have either never been used in the aeronautical field or have had other purposes, so in some cases it is necessary not to limit oneself to looking at data relating only to the aeronautical world.
Still referring to 4.2, it can be seen that the first four boxes are ticked, they indicate certain aircraft categories. In general, all acronyms beginning with A refer to aviation components, but of these only the first four are taken into account, because they indicate: aircraft in general, attack aircraft, fighter aircraft and inhabited aircraft. The other types, on the other hand, contain parts of both inhabited and uninhabited cargo aircraft, bombers and trainers. For more details, see the image below:

A	Airborne - The most generalized aircraft operation and testing conditions.
AA	Airborne Attack – General conditions for equipment installed on high performance aircraft such as used for ground support.
AF	Airborne Fighter – General conditions used for equipment installed in high performance aircraft such as fighters or interceptors.
AI	Airborne Inhabited - General conditions in inhabited areas without environmental extremes.
AIA	Airborne Inhabited Attack - Typical conditions in cargo compartments occupied by aircrew without environment extremes of pressure, temperature, shock and vibration and installed on high performance aircraft such as used for ground support.
AIB	Airborne Inhabited Bomber -Typical conditions in bomber compartments occupied by aircrew without environment extremes of pressure, temperature, shock and vibration and installed on long mission bomber aircraft.
AIC	Airborne Inhabited Cargo - Typical conditions in cargo compartments occupied by aircrew without environment extremes of pressure, temperature, shock and vibration and installed on long mission transport aircraft .
AIF	Airborne Inhabited Fighter - Typical conditions in cargo compartments occupied by aircrew without environment extremes of pressure, temperature, shock and vibration and installed on high performance aircraft such as fighters and interceptors.
AIT	Airborne Inhabited Transport - Typical conditions in cargo compartments occupied by aircrew without environment extremes of pressure, temperature, shock and vibration and installed on high performance aircraft such as trainer aircraft.
ARW	Airborne Rotary Wing - Equipment installed on helicopters; includes laser designators and fire control systems.
AT	Airborne Trainer – General conditions for equipment installed on high performance aircraft such as trainer aircraft.
AU	Airborne Uninhabited - General conditions of such areas as cargo storage areas, wing and tail installations where extreme pressure, temperature, and vibration cycling exist.
AUA	Airborne Uninhabited Attack - Bomb bay, equipment bay, tail, or where extreme pressure, vibration, and temperature cycling may be aggravated by contamination from oil, hydraulic fluid and engine exhaust. Installed on high performance aircraft such as used for ground support.
AUB	Airborne Uninhabited Bomber - Bomb bay, equipment bay, tail, or where extreme pressure, vibration, and temperature cycling may be aggravated by contamination from oil, hydraulic fluid and engine exhaust. Installed on long mission bomber aircraft.
AUC	Airborne Uninhabited Cargo – Equipment bay, tail, or where extreme pressure, vibration and temperature cycling may be aggravated by contamination from oil, hydraulic fluid and engine exhaust. Installed on long-mission transport aircraft.
AUF	Airborne Uninhabited Fighter - Bomb bay, equipment bay, tail, or where extreme pressure, vibration, and temperature cycling may be aggravated by contamination from oil, hydraulic fluid and engine exhaust. Installed on high performance aircraft such as fighters and interceptors.
AUT	Airborne Uninhabited Transport - Bomb bay, equipment bay, tail, or where extreme pressure, vibration, and temperature cycling may be aggravated by contamination from oil, hydraulic fluid and engine exhaust. Installed on high performance aircraft such as used for trainer aircraft.

Figure 4.3: NPRD filtre aeronautical types

Once the filters were defined, we proceeded with the search for the various components and to do this, we indicated the component in the 'part description' bar. Once the type of component was chosen, the window shows the various elements of the same family with their population, number of failures and the hours in which they were used (in millions of hours). The sum of the number of faults and hours is then shown at the bottom. All this is shown in the following image:

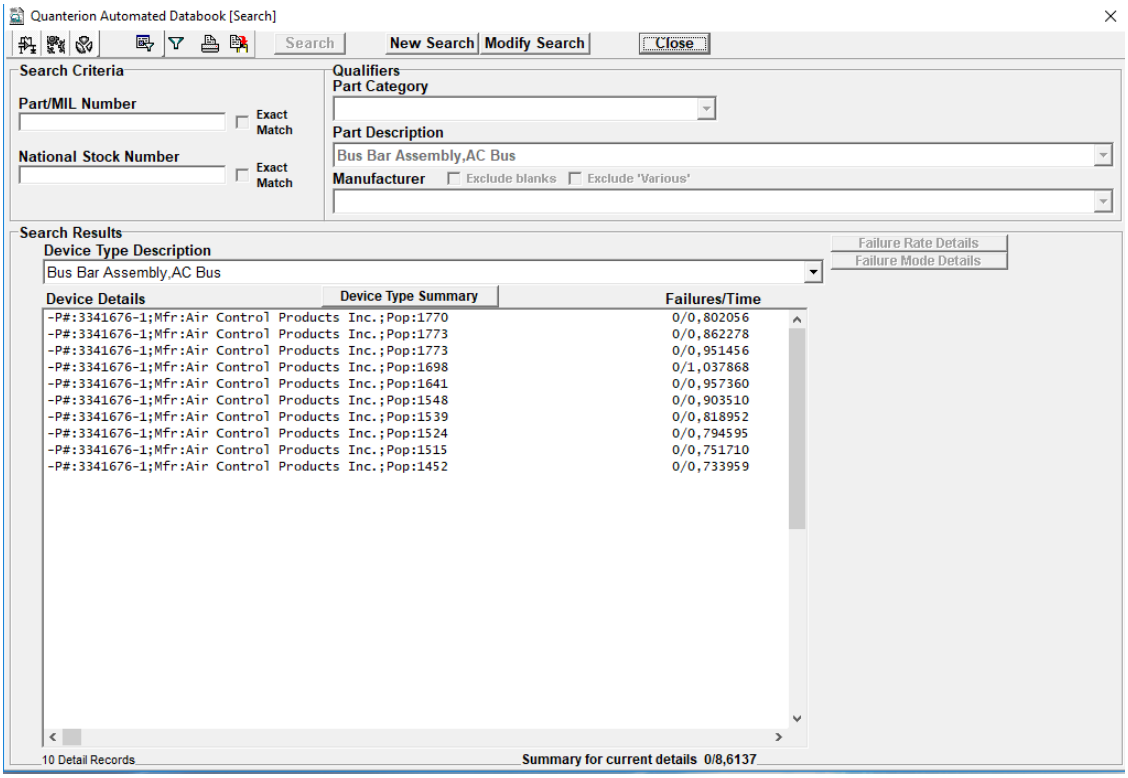

Figure 4.4: NPRD example page with the values

The data obtained, as written above, serve to obtain estimates by analogy between the components actually assumed for the various architectures and their real-life counterparts. This implies that the estimates obtained in the previous chapter will be more precise as the studies progress. However, even if the NPRD values are used as a first approximation of what they will be worth, their interpretation must seek to be as truthful as possible. In fact, to derive the failure rate, it is sufficient to divide the number of failures by the number of hours, but sometimes it is necessary to make probabilistic estimates on the data obtained.
It is sometimes the case that among the various components in a household, there are some that break down many more times than the overall average. In view of this, the following algorithm, suggested by Quaternion's own paper [40], was followed in estimating the failure rate: once the various components of the database are given, it is necessary to take into account how many there are, the number of the population, the number of failures and their number of hours, at this point if one does not have

too many components, simple division of the total value was considered sufficient, if there is no deviation in the average one proceeds equally with simple division, if one has many values and some parameters that deviate from the average one proceeded to use the CHI square method to exclude the values that alter the estimate.
Theoretically, one could also proceed with more in-depth statistical estimations, but since the elements taken into consideration often do not have a direct correspondence with the components that actually constitute the architectures under scrutiny, it was deemed sufficient to do as described above, so as also to avoid laborious estimations that often lead to minimal improvements.
Moreover, since most estimates are either based on a few values or have failure values in line with their average, the CHI Square method has rarely been used. It must also be said that often when used, the improvements in the estimate are not so great and given the complexity of the architectures, its impact is minimal. Consequently, it can be considered a good approximation to estimate the failure rate with simple division and to limit the statistical method of the CHI square only in cases where its use is strictly necessary, such as Switchers.

4.2 Data Analysis

4.2.1 Motors

Employed technology	**Failure Rate**	**Reliability**
Turbofan	$2{,}67{\cdot}10^{-6}$	0,999997
Turboshaft	$1{,}50{\cdot}10^{-5}$	0,999985
Turboprop	$1{,}50{\cdot}10^{-5}$	0,999985
Pistonprop	$3{,}13{\cdot}10^{-4}$	0,9997

Table 4.1: ≪Motors reliability≫ - 2023

The motor values were not taken from NPRD, but were obtained from web publications. This is because NPRD only reports components, with at most a few assemblies, and not values for complete systems. The motors in the analyses in the previous chapter have a dual purpose: either to serve as generators of power/thrust in the various architectures or to compare the analysed architectures with the actual ones. To do the latter, the fuel system values (given below) are needed to make the analysis as truthful as possible.
Turning to the table above, we read that the turbofan failure rate value [33]. This is based on a statistical estimate by the FAA. Of all the engines, it is the best. This is due to the simplicity of the engine architecture and because they are the ones mainly used for wight body aircraft, which have the most stinging regulations.
For the turboprop and turboshaft you have the same value. It too is derived from an FAA estimate [41]. It was decided to use the same failure rate because the two

engines are very similar to each other. The failure rate is an order of magnitude higher than that of the turbofan, because this architecture has more components, including a mechanical transmission to move the prope
ller, and consequently the probability of something going wrong is higher. Lastly, the pistonprop [33] has the highest failure rate of all, due to the nature of the engine, which is piston-driven and consequently more prone to failure, and to the fact that the development of these engines has remained virtually static over the last 30 years.

4.2.2 Fuel system

Employed technology	Failure Rate	Reliability
Pump	$1{,}49{\cdot}10^{-6}$	0,999998
Tank	$8{,}65{\cdot}10^{-8}$	0,99999991

Table 4.2: ≪Fuel system's parts reliability≫- 2023

To make the discussion as complete as possible, the analysis of the propulsion system would not be complete without any consideration of the fuel system. But in order not to burden the analysis, this system is examined by looking at just the two main components: the pumps and the tanks. Each engine/generator is connected to two pumps and two tanks, which, as we have seen, allows for multiple considerations in the RBD analysis.
As for the values of the failure rates, these were obtained from NPRD and are as shown in the table above. For both values, the failure rate was obtained by simple division between the number of failures and the number of hours and these values are derived from the application of the aviation filters described above.

4.2.3 Mechanical parts

Employed technology	Failure Rate	Reliability
Gearbox	$5{,}26{\cdot}10^{-6}$	0,999998
Freewheels	$6{,}09{\cdot}10^{-6}$	0,999994
Propeller Turbine	$1{,}13{\cdot}10^{-5}$	0,99998
Propulsor	$6{,}04{\cdot}10^{-6}$	0,999994

Table 4.3: ≪Mechanical parts reliability≫- 2023

This section lists the purely mechanical parts that the various architectures have, and they have all been derived from NPRD. These are not many, but of those shown in the table above, the most important is certainly the gearbox. This component is often placed between the current generator and the motor that generates power. Consequently, the gearbox has a safety critical importance, linked to the fact that due to its mass and complexity, an architecture does not have many of them. In

the cases examined (without considering MAXWELL, which does not have one, and STARC-ABL, which has a special configuration) they range from a minimum of two to a maximum of four. Its failure rate was derived by doing the simple division of the gearbox assembly, keeping the aero filters active.
Turning to the freewheel, its value was derived by doing the simple division of the item "Wheel Assembly" with the aero filters active and it is derived that there are 10 failures per one and a half million hours.
Propeller turbine sees the failure rate derived by doing the simple division of the entry "TURBINE,FAN" without the active filters as there were no values with the active filter. The reason for doing the simple division is that the number of failures is more or less stable considering the population analysed and the number of hours.
Finally, we have the propulsor which sees its value derived from the propeller entry by doing the simple division. No filters were used with the propeller entry, as no values were available with all active aircraft. Eventually, the value derived may not be entirely correct.

4.2.4 Electrical parts

Employed technology	**Failure Rate**	**Reliability**
Generator	$2{,}54{\cdot}10^{-6}$	0,999997
Magnetic Energy Storage	$7{,}61{\cdot}10^{-6}$	0,999992
Batteries	$9{,}31{\cdot}10^{-6}$	0,9999907
Fault Current Limiter	$1{\cdot}10^{-16}$	≈ 1
Switchers	$1{\cdot}10^{-10}$	≈ 1
AC Buses	$1{\cdot}10^{-16}$	≈ 1
DC Buses	$1{\cdot}10^{-16}$	≈ 1
Inverter	$7{,}06{\cdot}10^{-6}$	0,999993
Rectifer	$1{,}84{\cdot}10^{-5}$	0,99998
Electric Motor	$4{,}53{\cdot}10^{-6}$	0,999995
Control Modules	$2{,}79{\cdot}10^{-5}$	0,99997
Motor Controllers	$4{,}75{\cdot}10^{-6}$	0,999995
Take-off motors	$9{,}24{\cdot}10^{-6}$	0,9999907

Table 4.4: ≪Electrical parts reliability≫- 2023

The electrical components are those with the largest number of elements. Most of them are derived from study using NPRD, but some of them being electronic parts have no value in NPRD and consequently their values have been derived from studies relevant to the component itself and the architecture to which it belongs.
The first component in the list in the table 4.4 is the G enerator. Some of the architectures examined have the Superconducting Generator as a component, but in order to simplify the analysis, given that such components do not yet exist on the market, the value of the simple generator was also taken for them, effectively making an analogy. The failure rate is derived by simply dividing the 'Generator' item with

the active filters.
Next is the Magentic Energy Storage, its value is obtained by doing the simple division of the item "Storage Circuit Assembly" with the active filters. In this case, it was decided to do the simple division because there is not much data available on this.
Staying with the same family as the previous item, we have batteries. For their failure rate, the value derived from NPRD was not used, because this is derived exclusively from military aircraft and has a very high value ($1{,}73 \cdot 10^{-3}$) and is therefore completely insufficient for the architectures under consideration. Consequently, the value derived from [39] was taken, which is equal to $9{,}31 \cdot 10^{-6}$.
At this point on the table we have four components which have almost identical values: Fault Current Limiter, Switchers and AC/DC Buses. In fact, their failure rates are so low that their reliability is considered to be almost 1. For these values, the items without aeronautical filters have been taken into account because otherwise either no values are given or they are completely insufficient. It should be added that the analogy with commercially available elements has often been exploited for those components that are cryogenically cooled in some architectures.
Inverters have their failure rate value derived from the direct division of the item without active filters. In this case, the values derived from the use of filters could also be used, but these were considered insufficient and there were no failures. Consequently it was decided to be more conservative by using the general values. The same reasoning was then used for the Rectifer.
Moving on to electric motors, the situation that occurred with generators is repeated, where in some cases you have motors with superconductors. Here too, the value found on NPRD is continued by analogy. The value shown on the table was obtained using "MOTOR,AC: ALTERNATING CURRENT" without using filters, doing simple division. The CHI square method was also used, but since the improvement was on the order of one unit, it was decided to keep the previous value and be more conservative accordingly.
For the Control Modules, the simple calculation was simply carried out without filtering, as no values were available with the active filter.
Finally, we have the Motor Controllers and Take-off motors. These due to their particularity were not derived using NPRD, but directly from the document [39], which is a study on the reliability of certain MAXWELL components. In addition, this made it possible to verify part of the values derived from NPRD which are in line with what is reported here.

Chapter 5

Global Analysis

In this last chapter, attention is drawn to the significance of the results obtained in Chapter 3, trying to compare them not only with reference architectures, but also with each other, if they are for the same category of aircraft.
To do this, the various failure rates are shown in the table below:

Architecture	**Logistic RBD**	**Cruise RBD**	**Safety RBD**
2-engine Turbofan	$1{,}16{\cdot}10^{-5}$	$1{,}16{\cdot}10^{-5}$	$7{,}13{\cdot}10^{-12}$
2-engine Turboprop	$3{,}63{\cdot}10^{-5}$	$3{,}63{\cdot}10^{-5}$	$2{,}25{\cdot}10^{-10}$
2-engine Pistonprop	$6{,}32{\cdot}10^{-4}$	$6{,}32{\cdot}10^{-4}$	$9{,}79{\cdot}10^{-8}$
N3-X	3,37·10−4	$3{,}78{\cdot}10^{-5}$	$3{,}44{\cdot}10^{-9}$
SUGAR Volt	$5{,}35{\cdot}10^{-5}$	$1{,}16{\cdot}10^{-5}$	$2{,}28{\cdot}10^{-10}$
X-57 MAXWELL	$3{,}44{\cdot}10^{-4}$	$3{,}44{\cdot}10^{-4}$	$4{,}24{\cdot}10^{-9}(*)$
DRAGON Onera	$5{,}86{\cdot}10^{-4}$	$3{,}84{\cdot}10^{-5}$	$2{,}25{\cdot}10^{-10}$
STARC-ABL	$1{,}32{\cdot}10^{-4}$	$6{,}70{\cdot}10^{-5}$	$7{,}13{\cdot}10^{-12}$
PEGASUS NASA	$1{,}35{\cdot}10^{-4}$	$4{,}12{\cdot}10^{-5}(**)$	$8{,}67{\cdot}10^{-11}$

Table 5.1: ≪Architectures Failure Rate≫- 2023
*This is the value of when you can counteract the yawing moment with aerodynamic surfaces. The value if this moment is not counteracted is $7{,}44 \cdot 10^{-5}$.
**This is the value you would get with a hybridisation of 50% of cruising engines. In the case of a 25% hybridisation, this is based on that of the turboprop; in the case of a 75% hybridisation, the value is $6{,}44 \cdot 10^{-5}$.

Going into detail, referring to the table 5.1, the following considerations can be made:

- For logistic RBDs in general, the values are slightly worse than the reference architectures. The only exception is the X-57 MAXWELL which, having the pisrtonprop as a reference, is even better. This can be explained by the fact that the evolution of such engines over the past 30 years has not been much and at the regulatory level there have not been too many updates, while the MAXWELL having mainly electrical components has lower failure rates per ordinary component.
  Another that has a similar value to its benchmark is the SUGAR, which differs from the turbofan by only two units. While all others, which have the turbofan

as their reference, differ from it by an order of magnitude. This is because these architectures have more components than conventional ones, so the probability of failure is much higher.

- For the cruise, for simplicity's sake the reference architectures retain the value of the logistic since they have a simplified configuration compared to the real one. On the other hand, for the architectures under consideration, we see a general improvement in values compared to the logistic ones, and for some of them we have better values than the reference ones.
  Among these is N3-X which is slightly worse than the turbofan, this can be explained by the same concept behind the difference in the logistic, but its closeness to the reference value is due to the modularity that this architecture presents which can ensure the cruise with $\frac{3}{4}$ of working engines. This concept is reiterated when comparing the DRAGON. It is in fact the closest architecture to that of the N3-X. Its value is slightly worse because there are trivially more components.
  Turning to the SUGAR, this has the same value as the turbofan because in cruise it is the endothermic component that flies.
  Concluding the turbofan related architectures there is the STACR-ABL, this is the worst compared to the reference because basically its operational operation sees the turbofans acting as generators and the tail thruster providing the thrust, so as there are more components in series in operation there is a higher probability of failure.
  As for the MAXWELL, it was deemed appropriate to maintain the value of the logistic one due to the particular nature of the aircraft and this is not a problem as its failure rate is better than that of the pistonprop.
  Finally, the PEGASUS has a slightly worse value than the turboprop, but this is conditioned by the level of hybridisation of the engine. In fact, the value reported is the one with a hybridisation of about 50%, whereas if one were to consider that at 75%, one has $6.44 \cdot 10^{-5}$, which is even worse, although not by that much. But in addition to that one could consider a hybridisation of 25% and in that case one has the same value as the reference value. Determining which is the right value to consider is a function of the evolution the project will take.

- The last column shows the values of the analysis performed on the safety RBDs. Here, it is not possible to determine a general trend, so it is necessary to compare the various architectures on a case-by-case basis.
  N3-X can be regarded as the worst of all when compared with the reference

architecture, in fact between the two there are no less than three orders of magnitude of difference in favour of the turbofan. This can be explained by the fact that N3-X is, of all the architectures examined, the one with the greatest level of detail on the nature of the components used, and consequently there are many different failure rates to consider. In addition, it must be considered that almost all elements of this configuration are not currently available on the market, so the values of failure rates taken by association with existing components may not be entirely correct. Therefore, the value derived from N3-X is to be regarded as positive, since it requires further investigation depending on the development of the project and, above all, the elements comprising it.
Related to this is the DRAGON, which as already mentioned shares the design philosophy of the N3-X. It has a one unit better failure rate than the turbofan and this is explained by the same reasoning as the previous one, mainly the analysis had less variety of elements. But it is not just limited to this, in fact safety critical elements such as gearboxes here have been redundant and there are many more thrust generating motors. This as it turns out leads to a penalty in the logistic and cruise RBDs, but on the safety level it leads to very positive effects. Considering also the development of the various elements, there is room for improvement.
Continuing with aircraft that have turbofans as a reference, one has the STARC-ABL that has the same value as the reference one. This is because on a safety level this configuration can switch from turbo electric to conventional. This means that this architecture is the one most likely to be developed in the next few years (obviously if it is worthwhile in terms of performance and fuel consumption) because, in addition to being in line with current standards, it uses existing components and the aircraft can switch to the conventional configuration at any time.
The SUGAR has a failure rate that is two orders of magnitude higher; this is related to the nature of the RBD where the electric and endothermic parts are in series with each other, since the level of hybridisation is lower than 50%. Since endothermic engines are sized for the cruise phase only, on a safety level it is necessary to operate both parts, electric and thermal, to ensure maximum engine thrust. Of course, if only the thermal part is lost, the electric part can continue to be used, which improves reliability, albeit slightly. This does not detract from the fact that with the development of the electric component one can get closer to current standards, but one can hardly do better, given also the critical conditions in which the electric components have to survive.
For the MAXWELL, it was necessary to make two RBDs for safety. Due to the particular nature of the aircraft, which has cruise engines at the wing tips, it is not guaranteed that in the event of an OEI the yawing moment resulting from

the single operating engine can be compensated with the aerodynamic surfaces. If it can be counteracted, the failure rate is better than that of the pistonprop by an order of magnitude, for the usual reasons of electrical component reliability. If, on the other hand, it cannot be counteracted, a more conservative RBD is required, which leads to a failure rate three orders of magnitude worse than in today's engine and four orders of magnitude worse than in the other case examined. All this means that determining this aspect is of fundamental importance for the development of this architecture.
Finally, the PEGASUS proves to be among the safest architectures, since the failure rate is one order of magnitude better than the turboprop. This can be explained by the nature of the RBD, which basically sees the operation of 2 of the 4 engines used, regardless of whether they are hybrid-electric or full electric. Of course, it was taken into account by the theory that of the 2 out of 4 engines operating, these were not from the same side. In addition, further studies of this architecture and its elements are needed so that the value derived can be confirmed.

In conclusion, the analysis carried out indicates that the architectures developed in general are slightly worse than today's standards. But this alone is not sufficient, since certain aspects can undermine the security of such architectures. Consequently, further analyses are needed to confirm, if not improve, the estimates obtained in this thesis, making the models applied closer to reality, so that the results are also as true as possible.
Only then will it be possible to say whether the path taken is sustainable in terms of safety. But before that time, in addition to these studies, further analysis and research is needed to confirm that turbo/hybrid electric engines can guarantee the performance of engines currently on the market and that they can reduce greenhouse gas emissions and pollutants in their lifecycle, all at an affordable cost for airlines.

Chapter 6

Conclusions

From the study carried out, it emerges that turbo-electric engines, whatever their configuration, are the current technical challenge that the aviation sector must and will face in the coming years.
The studies analysed in Chapter 2 show that there is fervent research activity in this field throughout the world and, moreover, it is not only aimed at improving the technologies developed so far, something that has been done since the 1960s, but also seeks to innovate a sector (airliner flights) that does not lend itself well to radical innovations due (and rightly so) to safety regulations, with the aim, not only of economic, but also of reducing the emission of greenhouse gases that are causing global warming. Already now at the production level, the first aircraft of the 'more electric' philosophy are being put on the market. The most famous example is the Boeing 787 Dreamliner where engineers have managed to replace the pneumatic system with an electric one.
Going back to the previous lines, it is worth reiterating that the purpose of this study is to analyse the safety aspect of these propulsion architectures, so all reasoning related to performance and greenhouse gas emissions is eliminated. What is more, the study focused on those projects with a high level of progress in the realisation programme and with the aim of entering the market in the next few years.
Naturally, the level of detail among the various configurations analysed differs depending on the material available, as these projects are protected by the intellectual property of the various construction companies. Consequently, there are architectures with a higher level of detail than others.
While in general having a higher level of detail made it possible to find a more truthful failure rate for the architecture under analysis, it also led to the realisation of very large and complex RBDs. In addition to this, further analysis of the various architectures under consideration was required to understand how the aircraft behaved to the various failure modes that the configuration under analysis could have, which led in some cases to the realisation of multiple RBDs to cover more circumstances related either to the possibility of maintaining the flight envelope of

the aircraft under consideration, or more types of hybridisation of engines.
In general, it can be said that from the analysis carried out, the values obtained are generally positive, as they are often slightly worse than or close to the current reference architectures, and considering that further estimates are needed for those components that do not currently exist, these values can improve. But in addition to this, it is necessary to consider that in the analysis carried out, the engine cooling system was not taken into account. This system is safety critical and it would have been more appropriate to consider it in order to have the most accurate estimate possible. But the studies carried out on this system for the various architectures are few and consequently it was decided not to consider them due to the lack of data.
In conclusion, apart from this shortcoming, the values obtained for the various architectures are in line with what was expected, i.e. slightly worse results than those of today's architectures. Only time will tell whether these new technologies will be able to match or exceed current standards in terms of security.

Appendix A

RBD Configurations

This section explains the main configurations used for the definition of RBDs in Chapter 3.
Please note that the value of R is derived from the following expression (formula) where lambda is the failure rate.

A.1 CONVENTIONAL CONFIGURATIONS

A.1.1 Series Diagram

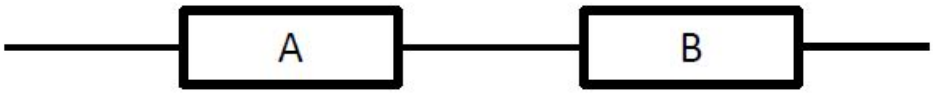

Figure A.1: Series Diagram

$$R_{series} = \prod_{i=1}^{n} R_i = R_A \cdot R_B \tag{A.1}$$

You have the blocks in series with each other, the overall R is given by the product of the blocks. The loss of one block leads to the loss of the system.

A.1.2 Parallel Diagram

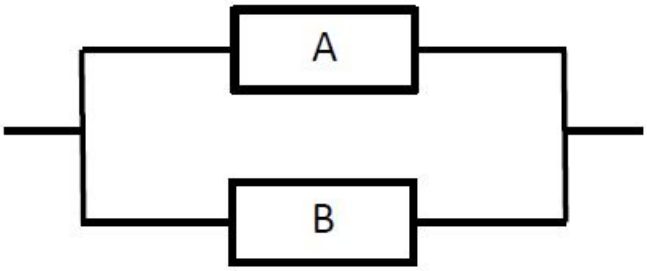

Figure A.2: Parallel Diagram

$$R_{parallel} = 1 - \prod_{i=1}^{n}(1 - R_i) = 1 - (1 - R_A) \cdot (1 - R_B) \tag{A.2}$$

You have the blocks in parallel with each other. This means that they are redundant, so the prediction of one block does not lead to the loss of the system, only the loss of the two blocks leads to the system not working.

A.2 UNCONVENTIONAL CONFIGURATIONS

In general, unconventional configurations can be said to exploit Bayes' method, i.e. the calculation of the overall R is carried out by solving several RBDs considering critical blocks either always working or never working.

A.2.1 H-pattern

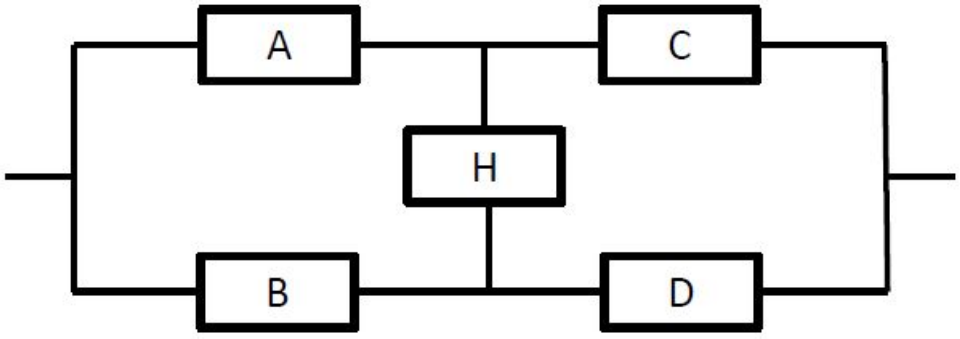

Figure A.3: H-pattern

$$R_{configurationH} = R_{partition1} \cdot R_{componentH} + R_{partition2} \cdot (1 - R_{componentH}) \quad \text{(A.3)}$$

In this case, we have that between two series in parallel there is an element that connects them. Consequently, the calculation of the reliability of the scheme is obtained by summing up the R obtained from the configuration with the communication element always working with the R of when this element does not work.
In case there are several components in the H-arm, their total R is calculated first and then the method is followed.

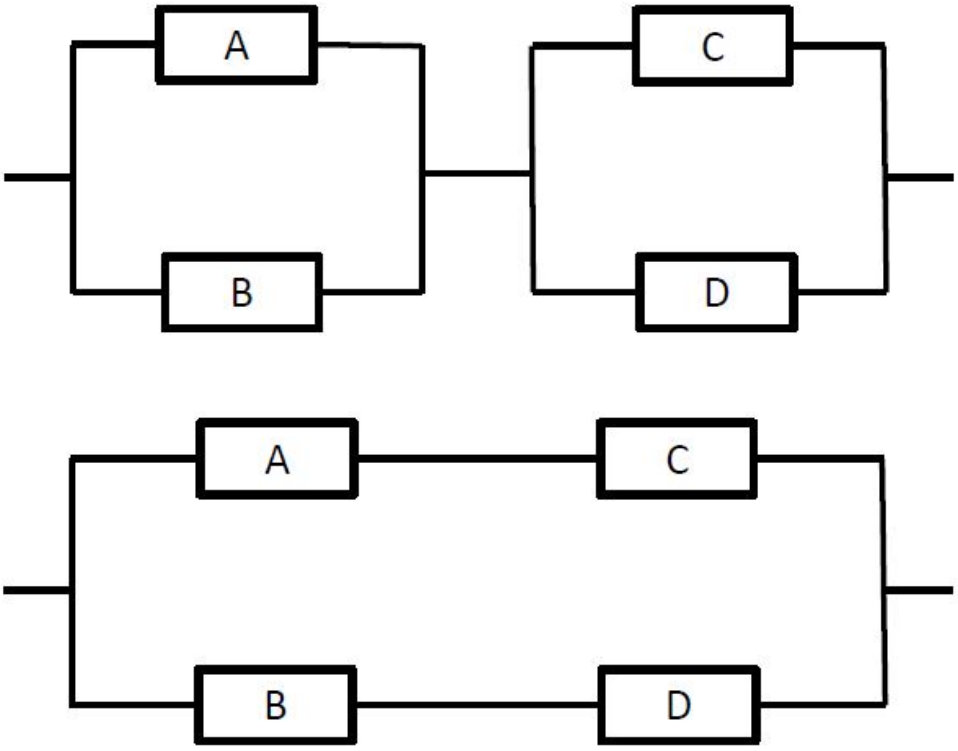

Figures A.4: H-pattern when the H component always works and when it doesn't

A.2.2 S-pattern

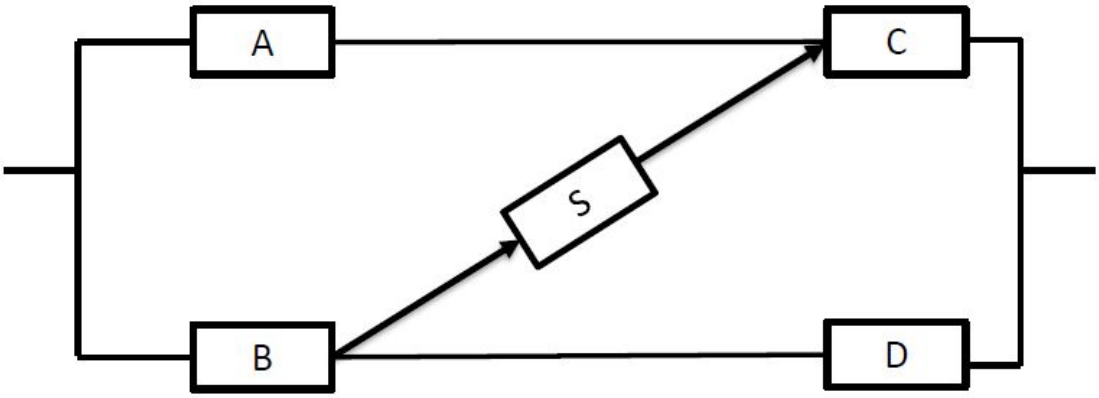

Figure A.5: S-pattern

$$R_S = AC + BD - ABCD + S(BC + ABCD - ABC - BCD) \tag{A.4}$$

Similar to the previous case, with the difference that the element connecting the two parallels can only be travelled in one direction and not in both directions like the H-element.

A.2.3 R-pattern

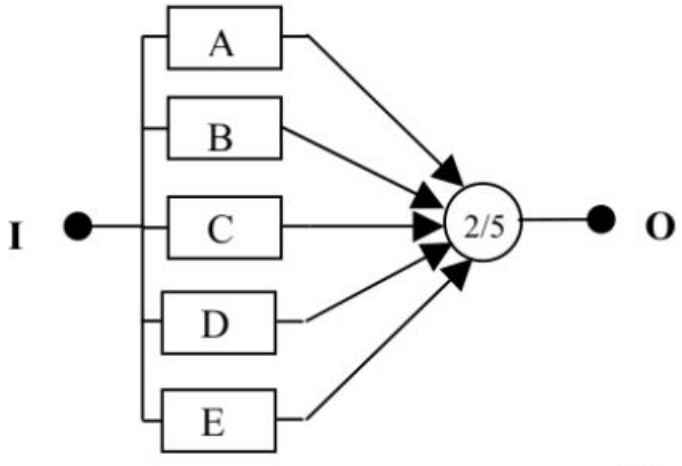

Figure A.6: R-pattern

$$\begin{aligned} F_S = &(1-R_A)\cdot(1-R_B)\cdot(1-R_C)\cdot(1-R_D)\cdot(1-R_E)+ \\ &(1-R_A)\cdot(1-R_B)\cdot(1-R_C)\cdot(1-R_D)\cdot R_E+ \\ &(1-R_A)\cdot(1-R_B)\cdot(1-R_C)\cdot R_D\cdot(1-R_E)+ \\ &(1-R_A)\cdot(1-R_B)\cdot R_C\cdot(1-R_D)\cdot(1-R_E)+ \\ &(1-R_A)\cdot R_B\cdot(1-R_C)\cdot(1-R_D)\cdot(1-R_E)+ \\ &R_A\cdot(1-R_B)\cdot(1-R_C)\cdot(1-R_D)\cdot(1-R_E) \end{aligned} \tag{A.5}$$

Where $R_S = 1 - F_S$.
This configuration has all elements in parallel but defines the minimum number of their operation. Its resolution sees two paths leading to the same result: either the probability of non-operation or the probability of operation is calculated. The scheme of the calculation is the same, either the cases in which the elements do not work or those in which they do work are considered, the only difference being that if one proceeds with the calculation of those that do not work, it is necessary to subtract 1 from the value obtained in order to obtain reliability. The choice of one way over another is a function of how long the calculation is.
In the event that the various blocks represent different elements, it is necessary to consider the various cases individually, but if the elements are the same, they can be grouped in the following way:

$$F_S = (1-R)^5 + 5\cdot R\cdot(1-R)^5 \tag{A.6}$$

The calculation of the numerical value is a function of the number of reference blocks and the S-number, which is the sum of 1 and the number of blocks not used as a reference:

$$N = \frac{n\cdot(n-1)\cdot(n-2)...(n-s+1)}{s!} \tag{A.7}$$

This concept can be made clearer by reading the application of this formula with an example. Consider an R-scheme of 12 elements all equal where only 8 are required to function. Then we have the following formula:

$$R_{tot} = R^{12}+12\cdot R^{11}\cdot(1-R)+66\cdot R^{10}\cdot(1-R)^2+220\cdot R^9\cdot(1-R)^3+495\cdot R^8\cdot(1-R)^4 \tag{A.8}$$

Taking the last numerical term as an example, it is derived:

$$495 = \frac{12 \cdot 11 \cdot 10 \cdot 9}{4!} \tag{A.9}$$

A.2.4 V-pattern

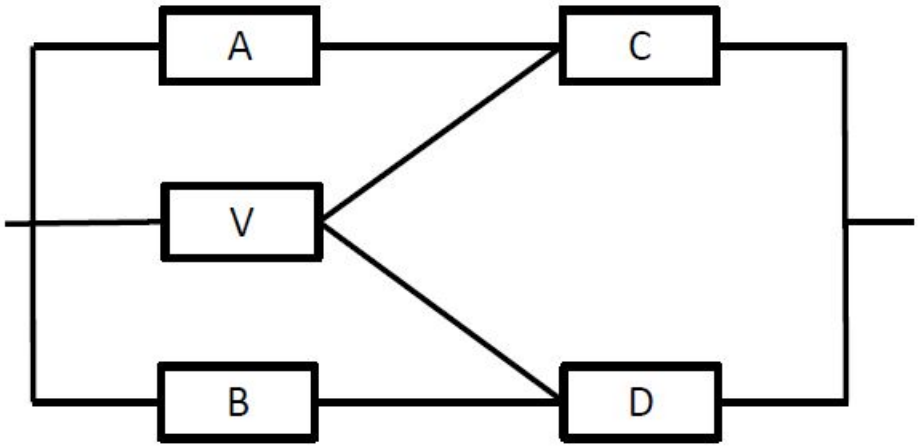

Figure A.7: V-pattern

$$R_{confV} = R_{partition1} \cdot R_{componentV} + R_{partition2} \cdot (1 - R_{componentV}) \tag{A.10}$$

Similar to the H- and S-scheme, in this case the reliability calculation is carried out considering whether the V-element works or not.

Bibliography

[1] B.Laumert. "Proposed Design and Feasibility Study of an Hybrid-Electric Propulsion System for a Ten Passenger Aircraft". In: *KTH School of Industrial Engineering and Management* (2019).

[2] S. Stückl. "Methods for the Design and Evaluation of Future Aircraft". In: *Technische Universität München* (2015).

[3] *Strategic research and innovation agenda*. 2020. URL: https://www.clean-aviation.eu/files/Clean_Aviation_SRIA_R1_for_public__consultation.pdf.

[4] Y. L. B. B. C. W. A. E. J. F. a. R. H.-R. Julian Hoelzen. *Conceptual Design of Operation Strategies for Hybrid Electric Aircraft*. 2018. URL: https://doi.org/10.3390/en11010217.

[5] M.Zafferetti. "Turbo-Electric propulsion system of a high bypass-ratio turbofan engine for civil liner airctaft". In: *Politecnico di Torino* (2018).

[6] Aerospace Technology. *E-Fan Electric Aircraft*. 2014. URL: https://www.aerospace-technology.com/projects/e-fan-electric-aircraft/.

[7] Pipistrel-Aircraft. URL: https://www.pipistrel-aircraft.com/taurus-g4-flies-at-the-nasa-gfc/.

[8] Emanuele Ferretti. *L'aereo "Alice" fully-electric e ad emissioni zero ha compiuto il primo volo con anche l'italiana MAGROUP impegnata nel progetto*. 2022. URL: https://www.aviation-report.com/aereo-fully-electric-alice-ha-compiuto-primo-volo-con-anche-italiana-magroup-impegnata-nel-progetto/.

[9] "Vola il prototipo di ZeroAvia con propulsione a idrogeno". In: *Aeronautica e Difesa* (mar. 2023).

[10] ZeroAvia. URL: https://www.zeroavia.com/.

[11] Sean Clarke; P.E.; Matthew Redifer; Kurt Papathakis e Aamod Samuel. *X-57 Power and Command System Design*. 2017. URL: https://ntrs.nasa.gov/api/citations/20170005797/downloads/20170005797.pdf.

[12] Donald L. Simon. *System-Level Control Concepts for Electrified Aircraft Propulsion Systems*. 2021. URL: https://ntrs.nasa.gov/api/citations/20210026284/downloads/TM-20210026284.pdf.

[13] C. D. J. H. R. L. M. R. I. C. O. A. C. F. B. P. Peter Schmollgruber. *Multidisciplinary Exploration of DRAGON: an ONERA Hybrid Electric Distributed Propulsion Concept*. 2019. URL: https://hal.archives-ouvertes.fr/hal-02068597.

[14] Peter Schmollgruber; David Donjat; Michael Ridel e Olivier Atinault Italo Cafarelli. "Multidisciplinary Design and performance of the ONERA Hybrid Electric Distributed Propulsion concept (DRAGON)". In: *AIAA Scitech 2020 Forum, Orlando, USA* (gen. 2020). URL: https://hal.science/hal-03125217.

[15] weflywright. URL: https://www.weflywright.com/.

[16] NASA. *Single-Aisle Turboelectric Aircraft with Aft Boundary Layer Propulsion (STARC-ABL)*. URL: https://www1.grc.nasa.gov/aeronautics/eap/airplane-concepts/starc-abl/.

[17] NASA. URL: https://www1.grc.nasa.gov/aeronautics/eap/airplane-concepts/n3x/.

[18] esaereo. URL: https://www.esaero.com/eco-150-project-information.

[19] IMOTHEP. URL: https://www.imothep-project.eu/main-results-27.

[20] ZUNUM Aero. URL: https://zunum.aero/technology/.

[21] Airbus. URL: https://www.airbus.com/en/innovation/zero-emission/electric-flight/e-fan-x.

[22] D. Kaminski-Morrow. *Airbus and Rolls-Royce cancel E-Fan X hybrid-electric RJ100 experiment*. 24/04/2020. URL: https://www.flightglobal.com/air-transport/airbus-and-rolls-royce-cancel-e-fan-x-hybrid-electric-rj100-experiment/138067.article.

[23] Rendón; M.A.; Sánchez R.; C.D.; Gallo M. *Aircraft Hybrid-Electric Propulsion: Development Trends, Challenges and Opportunities*. 2021. URL: https://doi.org/10.1007/s40313-021-00740-x.

[24] N. F. M. M. a. G. W. Mithun Eqbal. *Development of a Turbo Electric Distribution System for Remotely Piloted Aircraft Systems*. 2021. URL: https://doi.org/10.1590/jatm.v13.1209.

[25] C. D. S. R. J. G. M. a. A. H. A. Manuel A. Rendón. *Aircraft Hybrid-Electric Propulsion: Development Trends, Challenges and Opportunities*. 2021. URL: https://doi.org/10.1007/s40313-021-00740-x.

[26] F. W. a. M. P. Hendrik Gesell. "SYSTEM ANALYSIS OF TURBO ELECTRIC AND HYBRID ELECTRIC PROPULSION SYSTEMS ON A REGIONAL AIRCRAFT". In: *in 31st Congress of the International Council of the Aeronautical Science; Belo Horizonte; Brazil* (2018).

[27] C. Pornet. "Conceptual Design Methods for Sizing and Performance of Hybrid-Electric Transport Aircraft". In: *TECHNISCHE UNIVERSITÄT MÜNCHEN* (2017).

[28] W. KUCINSKI. *UTC's Project 804 hybrid-electric demonstrator may increase regional jet efficiency by 30 percent*. 2019. URL: https://www.sae.org/news/2019/04/utc%5C%E2%5C%80%5C%99s-project-804-hybrid-electric-demonstrator-may-increase-regional-jet-efficiency-by-30-percent.

[29] M. K. B. a. C. K. Droney. *Subsonic Ultra Green Aircraft Research: Phase II – Volume II – Hybrid Electric Design Exploration*. 2015. URL: https://ntrs.nasa.gov/citations/20150017039.

[30] Francisco M. Capristan e Nathaniel J. Blaesser. *Analysis of the Parallel Electric-Gas Architecture with Synergistic Utilization Scheme (PEGASUS) Concept*. 2019. URL: https://ntrs.nasa.gov/api/citations/20190030874/downloads/20190030874.pdf.

[31] *Commercial Aircraft Propulsion and Energy Systems Research Reducing Global Carbon Emissions*. 2016. URL: https://nap.nationalacademies.org/read/23490/chapter/7.

[32] Michael J. Armstrong; Mark Blackwelder; Andrew Bollman; Christine Ross; Angela Campbell; Catherine Jones e Patrick Norman. *Architecture, Voltage, and Components for a Turboelectric Distributed Propulsion Electric Grid Final Report*. 2015. URL: https://ntrs.nasa.gov/api/citations/20150014237/downloads/20150014237.pdf.

[33] Luca Piancastelli. *Powerplant Reliability Issues and Wear Monitoring in Aircraft Piston Engines. Part II: Engine Diagnostic*. 6/03/2018. URL: https://www.mdpi.com/2504-446X/2/1/10#B1-drones-02-00010.

[34] Australian Transport Safety Bureau. *Power plant failures in turbofan-powered aircraft*. 14/06/2014. URL: https://skybrary.aero/sites/default/files/bookshelf/3682.pdf.

[35] James L. Felder. *NASA N3-X with Turboelectric Distributed Propulsion*. 2015. URL: https://ntrs.nasa.gov/api/citations/20150002081/downloads/20150002081.pdf.

[36] Australian Transport Safety Bureau. *Power plant failures in turboprop-powered aircraft*. 15/06/2018. URL: https://www.atsb.gov.au/sites/default/files/media/5774415/ar-2017-017-final.pdf.

[37] AirShaper. *Electric Aviation - NASA interview on Maxwell X57 - Part 1: New Aerodynamic Concepts*. 2022. URL: https://www.youtube.com/watch?v=m4rysu8LlLM.

[38] Kevin R. Antcliff e Francisco M. Capristan. *Conceptual Design of the Parallel Electric-Gas Architecture with Synergistic Utilization Scheme (PEGASUS) Concept*. 2021. URL: https://ntrs.nasa.gov/api/citations/20210011499/downloads/Conceptual%5C%20Design%5C%20of%5C%20the%5C%20(PEGASUS)%5C%20Concept.pdf.

[39] Patrick R. Darmstadt; Ralph Catanese; Allan Beiderman; Fernando Dones; Ephraim Chen; Mihir P. Mistry; Brian Babie; Mary Beckman e Robin Preator. *Hazards Analysis and Failure Modes and Effects Criticality Analysis (FMECA) of Four Concept Vehicle Propulsion Systems*. 2019. URL: https://ntrs.nasa.gov/api/citations/20190026443/downloads/20190026443.pdf%20e%20https://doi.org/10.2514/6.2021-1723.

[40] Quanterion Solutions Incorporated. "Nonelectronic Parts Reliability Data". In: *NPRD databook* (2015).

[41] R.A. DeLucia; J.T. Salvino; B.C. Fenton. *Statistics on Aircraft Gas Turbine Engines Rotor Failures that Occurred on U.S. Commercial Aviation During 1985*. 7/1989. URL: https://www.tc.faa.gov/its/worldpac/techrpt/ct89-7.pdf.